Spring 2018 – Systems Biology of Reproduction
Discussion Outline – Male Reproductive Tract Development & Function
Michael K. Skinner – Biol 475/575
CUE 418, 10:35-11:50 am, Tuesday & Thursday
February 1, 2018
Week 4

Reproduction Tract Development & Function

Primary Papers:

1. Murashima, et al. (2015) Asian J Andrology 17:749-755
2. Okazawa, et al. (2015) Developmental Biology 400(1):139-47
3. Liu, et al. (2017) Sexual Development 11:190-202

Discussion

Student 7: Classic Reference 1 above

- What are the developmental steps of the Wolffian/epididymal duct?
- What are the Phenotypes of knockouts that explain the development?
- What technology was used

Student 8: Reference 2 above

- What is the technology used?
- Where is the expression pattern of the FGF receptor?
- What does the knockout phenotypes show on regional actions of FGF receptor?

Student 10: Reference 3 above

- What is the technology used?
- What androgen alterations in actin localization were observed?
- What basic information on male reproductive tract development was obtained?

[Downloaded free from http://www.ajandrology.com on Tuesday, January 19, 2016, IP: 134.121.42.92]

Asian Journal of Andrology (2015) 17, 749–755
© 2015 AJA, SIMM & SJTU. All rights reserved 1008-682X

www.asiaandro.com; www.ajandrology.com

Open Access

INVITED REVIEW

Sperm Biology

Understanding normal and abnormal development of the Wolffian/epididymal duct by using transgenic mice

Aki Murashima[1], Bingfang Xu[2], Barry T Hinton[2]

The development of the Wolffian/epididymal duct is crucial for proper function and, therefore, male fertility. The development of the epididymis is complex; the initial stages form as a transient embryonic kidney; then the mesonephros is formed, which in turn undergoes extensive morphogenesis under the influence of androgens and growth factors. Thus, understanding of its full development requires a wide and multidisciplinary view. This review focuses on mouse models that display abnormalities of the Wolffian duct and mesonephric development, the importance of these mouse models toward understanding male reproductive tract development, and how these models contribute to our understanding of clinical abnormalities in humans such as congenital anomalies of the kidney and urinary tract (CAKUT).

Asian Journal of Andrology (2015) **17**, 749–755; doi: 10.4103/1008-682X.155540; published online: 26 June 2015

Keywords: epididymis; mesonephros; transgenic mice; Wolffian duct

INTRODUCTION

Understanding the mechanisms that regulate the development of the Wolffian duct (WD) is important because disruption of epididymal function may arise as a consequence of its abnormal development. Very little is known of either the process of WD development or the nature and causes of congenital defects that lead to male infertility. For example, it is clear that an undeveloped initial segment of the epididymis leads to male infertility[1,2] and considering that the human epididymis has an initial segment-like epithelium,[3] it is important to at least understand the development of this region. There are three developmental processes that are considered to be important during the development of the WD: (1) mesonephros formation, (2) stabilization of the ductal system and further growth, (3) postnatal differentiation (**Figure 1**). Each process is dependent upon developmental factors as shown by WD phenotypic mice carrying mutations of each factor.

This review focuses on mouse models that display abnormalities in WD or mesonephric development, the importance of these mouse models toward understanding male reproductive tract development, and how these models contribute to understanding clinical abnormalities in humans. **Table 1** shows mutations of genes in mice that display Wolffian/epididymal duct phenotypes.

DEVELOPMENT OF WOLFFIAN/EPIDIDYMAL DUCT AND MOUSE MODELS

Mesonephros formation

During development, the nephric duct/Wolffian duct (WD) arises from the anterior, intermediate mesoderm, and extends caudally.[4] In the case of mouse, WD formation begins approximately on embryonic day (E) 8.5 and is completed by reaching the cloaca at E9.5[5] (**Figure 1a** and **1b**). As the WD elongates, it induces the formation of nephric tubules through a mesenchymal-epithelial transition process. The tubules form three kidney primordia: pronephros, mesonephros and metanephros[6] (**Figure 1c**). The pronephros and mesonephros are transient kidneys and degenerate soon after their formation. However, in the mesonephros, the WD and cranial mesonephric tubules (MT) are retained and give rise to the male reproductive tract including the epididymis and efferent ducts, respectively.

Because WD formation is crucial for kidney development in mammals, many mouse models that show abnormal WD or mesonephric development also display urogenital abnormalities. The paired domain transcription factors Pax2 and Pax8 are well-known inducers of the initial formation of the WD.[7,8] The LIM-class homeobox gene *Lim1* is required for the extension of the WD.[9,10] Mice carrying a null mutation of *Emx2*, a mouse homologue of the *Drosophila* head gap gene *empty spiracles* (*ems*), display normal WD development until E10.5, but at later time points the duct degenerates, resulting in lack of a kidney and a failure of the reproductive tract to develop.[11] Mice carrying a null mutation of *Gata3*, which is a transcriptional target of Pax2 and Pax8, also show defects in WD initiation.[12]

Growth factors can differentially regulate gene expression especially through epithelial-mesenchymal interactions. Fibroblast growth factor (FGF) signaling is one of the well analyzed growth factor signaling events during mesonephric formation. *Fgf8* encodes an FGF ligand, which is expressed in the intermediate mesoderm, and lack of its expression results in the absence of the cranial mesonephros and MTs.[13]

[1]Department of Developmental Genetics, Institute of Advanced Medicine, Wakayama Medical University, 811-1 Kimiidera, Wakayama 641-8509, Wakayama, Japan; [2]Department of Cell Biology, University of Virginia School of Medicine, Charlottesville, VA 22908, USA.
Correspondence: Prof. Barry T Hinton (bth7c@virginia.edu)
This article was presented at the 6th International Conference on the Epididymis in Shanghai, Oct 31-Nov 3, 2014.

[Downloaded free from http://www.ajandrology.com on Tuesday, January 19, 2016, IP: 134.121.42.92]

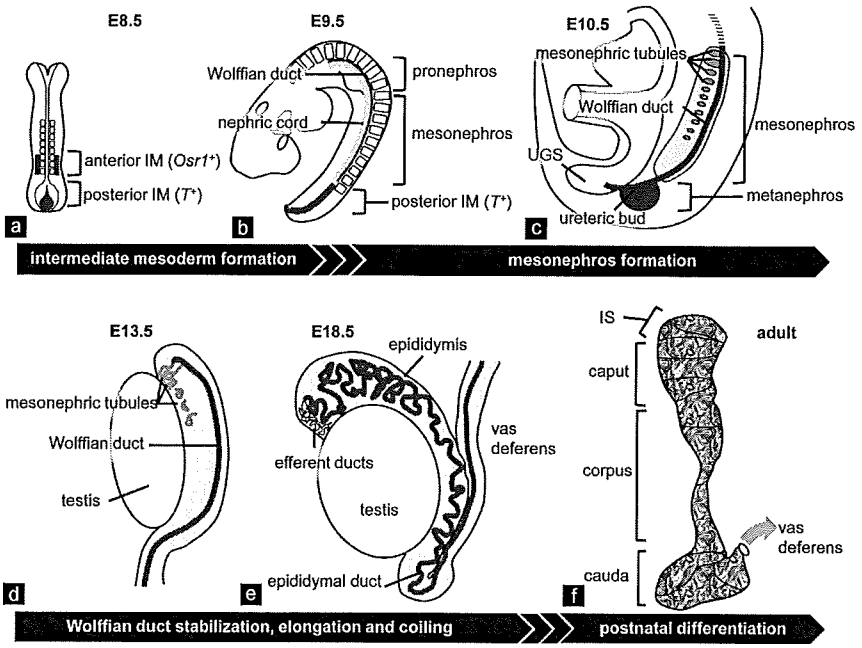

Figure 1: Schematic diagram of mouse Wolffian/epididymal duct development. (**a–c**) The origin of the epididymis is the intermediate mesoderm. Spatiotemporally distinct intermediate mesoderm at E8.5 gives rise to the WD and metanephric mesenchyme.[37] The anterior intermediate mesoderm, which gives rise to the pronephros and the whole WD, is composed of *Osr1*-positive cells at E8.5. The posterior intermediate mesoderm, which gives rise to the metanephric mesenchyme, is positive for *T* at E9.5. The posterior intermediate mesoderm may correspond to axial progenitor cells, which serve as the source of the caudal body trunk.[96,97] The WD begins to form from the anterior intermediate mesoderm at E8.5 and grows posteriorly reaching the urogenital sinus at E9.5.[98] Meanwhile, the pronephros regresses through apoptosis.[99] The WD induces the formation of mesonephric tubules from the mesenchyme (nephric cord) adjacent to the WD in a cranio-caudal manner. At the caudal end of the WD, the metanephros is initiated by ureteric bud formation through the interaction between WD epithelia and the metanephric mesenchyme at E10.5. (**d**) After gonadal sexual differentiation begins, the WD in the female embryo regresses from cranial to caudal while the WD in the male embryo is stabilized. The cranial set of mesonephric tubules connected to the WD is stabilized while the caudal set of mesonephric tubules regresses *via* apoptosis. (**e**) In the male embryo, the stabilized WD begins to coil from the cranial portion at E15.5. The duct continues to elongate and coil throughout development. (**f**) Ductal elongation and coiling continue after birth. The single-layered ductal epithelia undergo differentiation between P15 and P44. At the same time, the regions of the epididymis, initial segment, caput, corpus and cauda, become morphologically distinct. Sperm transport through the duct begins at approximately P35.[59,68] IM: intermediate mesoderm; UGS: urogenital sinus; IS: initial segment.

FGF ligands bind and activate alternatively-spliced forms of four tyrosine kinase FGF receptors (FGFRs 1–4).[14] During mesonephric development, *Fgfr1* is expressed in the mesenchyme while *Fgfr2* is in the epithelium, maintaining the WD and mesonephric mesenchyme.[15] The function of FGFR2 in the WD epithelia is suggested to maintain the caudal part of the WD in the mesonephros by regulating cell proliferation.[16]

Wnt genes encode a family of secreted glycolipoproteins regulating multiple processes during development, including cell proliferation and cell polarity. Among the *Wnt* genes, *Wnt9b* is mainly expressed in the WD epithelium while *Wnt7b* is faintly expressed from E9.5 onward. In animals devoid of *Wnt9b* their MTs are absent, and the epididymis is lacking at birth despite the normal formation of the WD at E10.5.[17] β-catenin-dependent canonical WNT signaling, which mainly regulates cell proliferation and differentiation, is sufficient to rescue MT induction in *Wnt9b* null mice. On the other hand, during metanephric kidney development, attenuation of *Wnt9b* affects the planar cell polarity of the epithelium and lead to tubules with an increased diameter.[18] Further spatiotemporal analyses of epididymal development in this mutant would contribute to our understanding of this molecule in tubulogenesis and its maintenance.

The number of MTs differs between species, and their function as a secretory organ is observed in pigs and humans but not in mice.[19–21] The number of efferent ducts reaching the testis also differs between species.[22,23] It is unclear whether there is a correlation between early MT number and the final number of efferent ducts observed in the adult. MT formation may resemble the formation of the renal nephron; both have the characteristic 'J' or 'S' shape during early development. The nephric tubule is formed through a mesenchymal-to-epithelial transition, and this cellular process is shared between mesonephric and metanephric tubules. *Pax2/8*, *Emx2* and *Lim1* are expressed in the condensed nephric cord and are required for tubulogenesis in addition to WD development.[7–11,24] The Wilms' tumor suppressor gene *Wt-1* and the homeobox gene *Six1* are also expressed in the nephrogenic mesenchymal condensation throughout the nephrogenic cord. Mice lacking *Wt-1* or *Six1* lack caudal MTs while cranial MTs are intact. These observations indicate that the regulation of the cranial and caudal set of MTs is distinct.[25–27] Conversely, lack of the forkhead transcription factors *Foxc1* and *Foxc2*, as well as *Sonic hedgehog* (*Shh*) expressed in the notochord or floor plate, results in supernumerary MT formation, suggesting suppressive effects of these genes on MT formation.[28,29] It is important to uncover how the differential regulation of tubule formation and stabilization along the anterior-posterior axis of the nephrogenic cord is established.

The connection between the rete testis and efferent ducts is observed at E13.5, and testicular fluid transport is detected at the corresponding stage of the rat embryo.[30] The patterning of efferent duct formation is intriguing, but the manner by which they reach the testis is not clear. There are at least two hypotheses on how the efferent ducts could be formed: (1) that a subset of MTs branch and fuse with each other forming the characteristic network of ductules, (2) that branching morphogenesis does not occur and the characteristic

[Downloaded free from http://www.ajandrology.com on Tuesday, January 19, 2016, IP: 134.121.42.92]

Table 1: Mouse models which show defects in WD/epididymal duct development

Gene	*Type of mutation, Cre driver*	*Phenotype of the mutant*	*References*
Defect in mesonephros formation			
Pax2	KO	Dysgenesis of WD and MD, absence of MT	7
Pax8	KO	Normal	24
Pax2/Pax8	dKO	Dysgenesis of WD and MD, absence of MT	8
Lim1	KO	Dysgenesis of WD	10
	Pax2-Cre	Defect in caudal WD extension	9
Gata3	KO	Dysgenesis of WD and MD, absence of MT	12
Wt-1	KO	Absence of caudal MT	26
Six1	KO	Absence of caudal MT	27
Osr1	KO	Defect in WD extension, absence of MT	100
Emx2	KO	Regression of whole WD	11
Wnt9b	KO	Absence of MT, absence of epididymis	17
Fgf8	*T-Cre*	Regression of cranial mesonephros	13
Fgfr1/2	*T-Cre*	Dysgenesis of WD and MT	13
	Pax3-Cre	Absence of MT	15
Fgfr2	*Hoxb7-Cre*	Regression of caudal WD	16
Shh	KO	Numerous ectopic MT, ectopic UB	29
Foxc1/2	*Foxc1/Mf1^{ch}*, KO	Numerous ectopic MT, ectopic UB	28, 101
c-ret	*ret-k^{-}*	Reduced number of MT	102
Raldh2	KO	Absence of WD	103
Lfng	KO	Blockage of the connection between efferent duct and rete testis	36
Defects in WD stabilization, elongation and coiling			
Ar	*Tfm*, KO	WD regression	40,41
Inhba	KO	Failed to develop ductal coiling in epididymis	53
Sfrp1/2	dKO	Shortened vas deferens	56
Vagl2	*Vangl2$^{lp/lp}$*	Shortened vas deferens	56
Wnt5a	KO	Shortened vas deferens	56
Pkd1	KO, *Pax2-Cre*	Coiling defect, cystic dilation of efferent ducts	54
Defects in postnatal differentiation			
Pten	*Rnase10-Cre*	Dedifferentiation of IS	2
Ros1	KO	Undifferentiated IS	1
Dusp6	KO	Large caput and corpus	67
Frs2	*Hoxb7-Cre*	Morphologically normal	68
	Rnase10-Cre	Abnormal shape of epididymis	68
Ar	*Ap2a-Cre*	Defective epithelial cell differentiation	47
	Rnase10-Cre	Absence of IS, defective epithelial cell differentiation	70
	FoxG-Cre	Absence of IS, defective epithelial cell differentiation	71
	Probasin-Cre	Small epididymis and seminal vesicle	69
Dicer	*Defb4-Cre*	Epithelial cell dedifferentiation	75
miR-29a	*miR-29b1^{UBC}* transgene	Hypoplastic epididymis	77
Lgr4	*Lgr4$^{Gt/Gt}$*	Short, dilated and much less convoluted epididymal ducts	104
	KO	Blockage of efferent duct	105
Shp1	*mev/mev*	Aberrant epididymal region	66
Hoxa11	KO	Transformation of vas deferens to epididymis	79
Hoxa10	KO	Transformation of vas deferens to epididymis	80

WD: wolffian duct; MT: mesonephric tubules; UB: ureteric bud; IS: initial segment; MD: mullerian duct

network of ductules is formed by simple fusion of a subset of MTs. The latter hypothesis would seem more feasible than the first because of the presence of blind-ended tubules. These MTs only fuse to one other MT, leaving one end sealed, hence becoming blind-ended. Obviously, there must be considerable coordination between the fusion events that limit the number of MTs that can fuse[4,5] resulting in the conus (2–3 fused MTs) and the single common ductule.[22] Identification of the genes and processes by which the formation and patterning of the efferent ducts occur is crucial, and the GUDMAP *in situ* hybridization database (http://www.gudmap.org/index.html)[31,32] clearly shows some potential genes that may regulate their formation, e.g., collagen triple helix repeat containing 1*(Cthrc1)*, cortexin 3 *(Ctxn3)* and laminin, alpha1 *(Lama1)*. *Lunatic fringe* (*Lfng*) is one of the mammalian *fringe* genes encoding a modifier of the notch receptor expressed in the developing WD, MTs and testis.[33–35] *Lfng*-null mice show partial bilateral blockage of the connection between the rete testis and the efferent ducts, indicating the involvement of notch signaling in establishing the rete testis-efferent duct boundary.[36]

The origins of nephron progenitor cells are suggested to differ between mesonephros and metanephros.[37] Metanephric mesenchyme is

[Downloaded free from http://www.ajandrology.com on Tuesday, January 19, 2016, IP: 134.121.42.92]

derived from a posterior immature caudal population, which is positive for *Brachyury* (*T*) expression, and persists in the posterior end of the embryo until body axis extension is complete (**Figure 1a**). On the other hand, the WD and at least part of the mesonephric mesenchyme arise from the anterior intermediate mesoderm, which is defined by *Osr1* expression at E9.5 (**Figure 1b**). These recent studies may indicate that abnormal body axis extension affects the intermediate mesodermal cell fate. It is possible that disruption of the A-P body axis extension affects not only the metanephric mesenchyme but also the mesonephric mesenchymal distribution, and subsequently further male reproductive tract development. Conditionally-induced mutations of the planar cell polarity (PCP) pathway-related genes, *Wnt5a*, *Ror2* and *Vangl2*, which are important for A-P body axis extension, demonstrate that insufficient A-P axis extension of the posterior intermediate mesoderm is correlated with urogenital tract abnormalities.[38] It is clear that more studies are needed to examine the early formation of the intermediate mesoderm and how this translates into development of the WD.

Stabilization of the ductal system and further growth: elongation and coiling

During embryogenesis, the mesonephros gives rise to a stable male reproductive tract whereas the mesonephros in the female regresses (**Figure 1d** and **1e**). Androgens produced in the testis are a major factor regulating this stabilization.[39–42] Following gonadal sex differentiation, the testis begins to produce the androgen, testosterone, at approximately E12.5.[43,44] Unlike for other androgen-dependent organs, such as the prostate and seminal vesicle, it has been suggested that locally-produced, and not systemic androgen, from the testis is necessary for WD stabilization.[45] Indeed, fluorescence labeling of an androgen ligand shows that androgen is transported within the luminal fluid.[30] However, there are studies showing that testicular androgen delivered via the systemic circulation is sufficient to prevent WD regression. Subcutaneous testicular grafts stabilize the WD in female marsupial embryos.[46] Androgens act through the androgen receptor (AR), a member of the nuclear receptor superfamily. The expression of AR is mainly detected in the mesenchyme surrounding WD epithelia at E13.5 in the mouse. Tissue-specific *Ar* knockout (KO) analyses demonstrate that WD stabilization and coiling is induced in the absence of epithelial-expressed *Ar*, demonstrating the importance of *Ar* in the mesenchyme.[47] This finding is consistent with the observation from tissue recombination experiments on androgen-insensitive *Testicular feminized* (*Tfm*) mice.[48,49] Several growth factors, including FGF and Epidermal growth factor (EGF), are suggested to mediate androgen functions in the prostate and WD.[50–52] However, the molecular mechanisms by which androgens regulate these genes *in vivo* are not known.

To create a long, highly-convoluted epididymal duct, the WD begins to elongate and coil from E15.5, following stabilization (**Figure 1e**). This process is also androgen-dependent, but growth factor signaling has been reported to regulate this elongation event. Tomaszewski *et al.* reported that *Inhba*, a subunit of both inhibins and activins, is a regional paracrine factor in mouse mesonephroi that controls coiling of the epithelium in the anterior WD.[53] *Pkd1*, whose mutation accounts for 85% of autosomal dominant polycystic kidney disease, and is a membrane-spanning glycoprotein involved in growth factor signaling transduction and cytoskeleton dynamics. Epithelial coiling is absent from the *Pkd1* mutant.[54] In both mutations, epithelial cell proliferation is attenuated. Recently, mathematical modeling has suggested that epididymal tubule morphogenesis is dependent upon the cell proliferation area in the tubule and mechanical resistance from the tissues surrounding the tubule.[55]

The secreted frizzled-related proteins (SFRPs) antagonize WNT ligand protein binding to its receptor FZD. The double KO (dKO) of *Sfrp1* and *Sfrp2* genes results in a shortened WD and vas deferens.[56] Androgen administration to these animals never rescues this phenotype, indicating that the abnormalities in *Sfrp1/2* dKO mutant male embryos are not caused by insufficient production of testosterone from the testes, but may reflect insensitivity of some target tissues to androgens.[56] It is also possible to consider that these phenotypes are, at least partially, a secondary consequence of the A-P extension defect of intermediate mesoderm formation described above. Although recent analyses have partially revealed the molecular mechanisms of ductal morphogenesis, further analyses should be performed including how androgen signaling regulates these molecules.

Postnatal differentiation: regional differentiation and epithelial cell differentiation

The epididymis consists of distinct anatomical regions that vary between species. However, in the mouse four regions can be defined: initial segment and caput, corpus and cauda epididymidis (**Figure 1f**). Each region is further divided into many segments characterized by expression of specific mRNAs, proteins and a repertoire of cell types.[57,58] The segments, divided by septa, are observed after birth and are distinct during puberty, postnatal (P) days 14–35. Impaired epididymal regionalization or epithelial cell differentiation results in male infertility. For example, if the initial segment does not develop, then male infertility results. Data from efferent duct ligation (EDL) experiments suggested that luminal fluid coming from testis is responsible for the maintenance of initial segment cell survival, proliferation and differentiation.[59,60]

Several growth factors, including FGFs 2,4 and 8, are detected in testicular fluid, and *Fgfrs* are expressed in the epithelium of the initial segment.[61,62] During normal development, high activity of the MAPK pathway, especially p-MAPK1/3 (p-ERK1/2), is detected in the initial segment.[60] EDL abolishes their activities, emphasizing the importance of lumicrine factors regulating their activity.[60] *Ros1* encodes an orphan receptor tyrosine kinase that is expressed in few epithelia, among them the WD and its derivatives.[63–65] Loss of *Ros1* expression or a naturally-occurring mutation of *Shp1* (*me*^{v}), a negative regulator of ROS1, results in abnormal differentiation of the initial segment.[1,66] *RNase10-Cre* drives gene recombination in the initial segment epithelia from P17 onward. *RNase-Cre*-mediated mutation in *Pten*, a negative regulator of PIP3/AKT signaling, induces dedifferentiation of the initial segment.[2] In these animals, abnormal differentiation results in an abnormally shaped initial segment. MAPK signaling regulators such as DUSP6 and FRS2 play important roles in epididymal cell proliferation and survival during postnatal development.[67,68]

Androgens are important regulators of epididymal development from embryonic to adult stages. From later stages of development to the adult stage, *Ar* expression in the epithelia is greater than that in the mesenchyme. Several *Ar* KO mice have been reported, and the majority show a hypoplastic epididymis and defective epithelial cell differentiation.[47,69–71] A differentiated epididymal epithelium is pseudostratified and comprises principal, clear, narrow, basal and recently-identified dendritic cells throughout the duct.[72,73] Similar to other pseudostratified epithelia, for example the trachea, the epididymal luminal environment regulates secretion and absorption of ions, water, organic solutes and proteins.[74] The molecular mechanisms of epididymal epithelial differentiation are not clear. Chimeric mutation of the *Ar* indicates that defective epithelial cell differentiation is cell-autonomous.[47] Dicer and small RNAs also regulate epididymal

[Downloaded free from http://www.ajandrology.com on Tuesday, January 19, 2016, IP: 134.121.42.92]

development and epithelial cell differentiation partially through androgen action.[75–77]

Hox genes are evolutionarily-conserved transcriptional regulators that determine body patterning.[78] As found for body plan formation, vertebrae and the gut, *Hox* genes, *Hoxa10* and *Hoxa11* are suggested to determine the boundary between the epididymis and vas deferens.[79–81] Later studies by Snyder *et al.*[82] showed that there were additional region-specific (efferent ducts, epididymis and vas deferens) *Hox* transcripts that may define boundaries along the reproductive tract during development.

POSSIBLE CONTRIBUTION OF MOUSE MODELS TO UNDERSTAND HUMAN CINICAL ABNORMALITIES

One of the most well-known congenital anomalies of the epididymis or vas deferens is congenital bilateral absence of the vas deferens (CBAVD). It occurs in 1%–2% of men with infertility.[83] 60%–90% of the CBAVD men harbor at least one associated *cystic fibrosis transmembrane conductance regulator* (*CFTR*) gene mutation.[84] 10%–40% of CBAVD men do not have recognizable *CFTR* gene abnormalities accompanied by unilateral renal agenesis (URA).[85] Presumably, CBAVD patients have disrupted morphogenesis of the early mesonephros owing to the mutation of genes.[86] Those genes involved in mesonephros formation, e.g., *Pax2*, *Wt-1* and *Fgfs*, may be viable candidate genes responsible for CBAVD with renal malformation.

Conversely, congenital anomalies of kidney and urinary tract (CAKUT) often carry mutations in genes, such as *PAX2* and *WT-1*, and male mice carrying mutations of these genes also exhibit reproductive tract malformations.[87] Syndromes with renal tract abnormalities also carry mutations in the genes described above. Branchio-Oto-Renal (BOR) syndrome is a genetic condition that typically disrupts the development of tissues in the neck and causes malformations of the ears and kidneys. *EYA1*, the human homolog of the *Drosophila eyes absent* gene, is the most common gene responsible for BOR.[88] Further, *Foxc1* regulates *Eya1* expression.[28] Mutations in the *SIX1* gene can be detected in 2% of individuals with the clinical diagnosis of BOR.[89] Mutations in both *ROR2*[90] and *WNT5A*[91] have been implicated in a rare genetic disease, Robinow syndrome, which exhibits several defects such as dwarfism, hydronephrosis and genital abnormalities. Because these syndromes often exhibit lethal abnormalities, it is still unclear if these mutations affect male fertility in humans.

Epididymal disjunction is the failure of the efferent ducts to reach the testis, which may reflect the failure of the efferent ducts to elongate, and presumably coil, during their development.[92–95] Interestingly, one study[95] has shown that 30%–79% of boys with an undescended testis also have Wolffian duct abnormalities, of which 25% display epididymal disjunction. Therefore, it is important that epididymal abnormalities be detected at orchidopexy, or other male infertility, which may be classified as idiopathic, will result. As mentioned above, it is not clear how the efferent ducts form, elongate, are directed toward the testis and then fuse with the rete testis. Obviously, mouse models that display epididymal disjunction will greatly aid our understanding of this abnormality.

SUMMARY

One of the striking characteristics of the epididymis is its complex developmental process. The primordium of the epididymis, the mesonephros, arises as a part of the transient kidney, and its stability and differentiation are regulated by hormonal signaling including by androgens and growth factors. In human, it transforms its morphology to form a 6 m duct that is coiled and packed into a three-dimensional organ of approximately 10 cm in length. Recent studies utilizing a variety of transgenic mice have revealed the molecular contribution of numerous factors at each stage of epididymal development. The molecular dissection of the developmental mechanisms of the epididymis has just begun. Integrative understanding of the hierarchy and interaction of each factor will provide new directions in this field. Considering that the epididymis shares its origin with the urinary tract, it is noteworthy that the molecular mechanisms which lead to kidney mal-development, such as CAKUT, may provide significant insight for the mesonephros derivative mal-development, such as CBAVD and *vice versa*.

COMPETING FINANCIAL INTERESTS

Neither author declares a competing interest.

ACKNOWLEDGMENTS

We would like to thank Prof. Gen Yamada and Dr. Mika Okazawa for the supportive discussion. This work is supported by Grant-in-Aid for Young Scientists B (25860771), and National Institutes of Health Eunice Kennedy Shriver NICHD Grants HD069654 and HD068365 (BTH).

REFERENCES

1 Sonnenberg-Riethmacher E, Walter B, Riethmacher D, Gödecke S, Birchmeier C. The c-ros tyrosine kinase receptor controls regionalization and differentiation of epithelial cells in the epididymis. *Genes Dev* 1996; 10: 1184–93.
2 Xu B, Washington AM, Hinton BT. PTEN signaling through RAF1 proto-oncogene serine/threonine kinase (RAF1)/ERK in the epididymis is essential for male fertility. *Proc Natl Acad Sci U S A* 2014; 111: 18643–8.
3 Yeung CH, Cooper TG, Bergmann M, Schulze H. Organization of tubules in the human caput epididymidis and the ultrastructure of their epithelia. *Am J Anat* 1991; 191: 261–79.
4 Atsuta Y, Tadokoro R, Saito D, Takahashi Y. Transgenesis of the Wolffian duct visualizes dynamic behavior of cells undergoing tubulogenesis *in vivo*. *Dev Growth Differ* 2013; 55: 579–90.
5 Staack A, Donjacour AA, Brody J, Cunha GR, Carroll P. Mouse urogenital development: a practical approach. *Differentiation* 2003; 71: 402–13.
6 Saxen, L. Organogenesis of the Kidney. Cambridge University Press; 1987.
7 Torres M, Gómez-Pardo E, Dressler GR, Gruss P. Pax-2 controls multiple steps of urogenital development. *Development* 1995; 121: 4057–65.
8 Bouchard M, Souabni A, Mandler M, Neubüser A, Busslinger M. Nephric lineage specification by Pax2 and Pax8. *Genes Dev* 2002; 16: 2958–70.
9 Pedersen A, Skjong C, Shawlot W. Lim 1 is required for nephric duct extension and ureteric bud morphogenesis. *Dev Biol* 2005; 288: 571–81.
10 Kobayashi A, Shawlot W, Kania A, Behringer RR. Requirement of Lim1 for female reproductive tract development. *Development* 2004; 131: 539–49.
11 Miyamoto N, Yoshida M, Kuratani S, Matsuo I, Aizawa S. Defects of urogenital development in mice lacking Emx2. *Development* 1997; 124: 1653–64.
12 Grote D, Souabni A, Busslinger M, Bouchard M. Pax2/8-regulated Gata 3 expression is necessary for morphogenesis and guidance of the nephric duct in the developing kidney. *Development* 2006; 133: 53–61.
13 Kitagaki J, Ueda Y, Chi X, Sharma N, Elder CM, *et al.* FGF8 is essential for formation of the ductal system in the male reproductive tract. *Development* 2011; 138: 5369–78.
14 Ornitz DM, Itoh N. Fibroblast growth factors. Genome Biol. 2001;2(3):REVIEWS3005. Epub 2001 Mar 9. Review.
15 Poladia DP, Kish K, Kutay B, Hains D, Kegg H, *et al.* Role of fibroblast growth factor receptors 1 and 2 in the metanephric mesenchyme. *Dev Biol* 2006; 291: 325–39.
16 Okazawa M, Murashima A, Harada M, Nakagata N, Noguchi M, *et al.* Region-specific regulation of cell proliferation by FGF receptor signaling during the Wolffian duct development. *Dev Biol* 2015; 400: 139–47.
17 Carroll TJ, Park JS, Hayashi S, Majumdar A, McMahon AP. Wnt9b plays a central role in the regulation of mesenchymal to epithelial transitions underlying organogenesis of the mammalian urogenital system. *Dev Cell* 2005; 9: 283–92.
18 Karner CM, Chirumamilla R, Aoki S, Igarashi P, Wallingford JB, *et al.* Wnt9b signaling regulates planar cell polarity and kidney tubule morphogenesis. *Nat Genet* 2009; 41: 793–9.
19 de Martino C, Zamboni L. A morphologic study of the mesonephros of the human embryo. *J Ultrastruct Res* 1966; 16: 399–427.
20 Tiedemann K, Egerer G. Vascularization and glomerular ultrastructure in the pig mesonephros. *Cell Tissue Res* 1984; 238: 165–75.
21 Smith C, Mackay S. Morphological development and fate of the mouse mesonephros. *J Anat* 1991; 174: 171–84.

[Downloaded free from http://www.ajandrology.com on Tuesday, January 19, 2016, IP: 134.121.42.92]

22 Guttroff RF, Cooke PS, Hess RA. Blind-ending tubules and branching patterns of the rat ductuli efferentes. *Anat Rec* 1992; 232: 423–31.
23 Ilio KY, Hess RA. Structure and function of the ductuli efferentes: a review. *Microsc Res Tech* 1994; 29: 432–67.
24 Mansouri A, Chowdhury K, Gruss P. Follicular cells of the thyroid gland require Pax8 gene function. *Nat Genet* 1998; 19: 87–90.
25 Kreidberg JA, Sariola H, Loring JM, Maeda M, Pelletier J, *et al.* WT-1 is required for early kidney development. *Cell* 1993; 74: 679–91.
26 Sainio K, Hellstedt P, Kreidberg JA, Saxén L, Sariola H. Differential regulation of two sets of mesonephric tubules by WT-1. *Development* 1997; 124: 1293–9.
27 Kobayashi H, Kawakami K, Asashima M, Nishinakamura R. Six1 and Six4 are essential for Gdnf expression in the metanephric mesenchyme and ureteric bud formation, while Six1 deficiency alone causes mesonephric-tubule defects. *Mech Dev* 2007; 124: 290–303.
28 Kume T, Deng K, Hogan BL. Murine forkhead/winged helix genes Foxc1 (Mf1) and Foxc2 (Mfh1) are required for the early organogenesis of the kidney and urinary tract. *Development* 2000; 127: 1387–95.
29 Murashima A, Akita H, Okazawa M, Kishigami S, Nakagata N, *et al.* Midline-derived Shh regulates mesonephric tubule formation through the paraxial mesoderm. *Dev Biol* 2014; 386: 216–26.
30 Tong SY, Hutson JM, Watts LM. Does testosterone diffuse down the Wolffian duct during sexual differentiation? *J Urol* 1996; 155: 2057–9.
31 Harding SD, Armit C, Armstrong J, Brennan J, Cheng Y, *et al.* The GUDMAP database – an online resource for genitourinary research. *Development* 2011; 138: 2845–53.
32 McMahon AP, Aronow BJ, Davidson DR, Davies JA, Gaido KW, *et al.* GUDMAP: the genitourinary developmental molecular anatomy project. *J Am Soc Nephrol* 2008; 19: 667–71.
33 Johnston SH, Rauskolb C, Wilson R, Prabhakaran B, Irvine KD, *et al.* A family of mammalian Fringe genes implicated in boundary determination and the Notch pathway. *Development* 1997; 124: 2245–54.
34 Lupien M, Diévart A, Morales CR, Hermo L, Calvo E, *et al.* Expression of constitutively active Notch1 in male genital tracts results in ectopic growth and blockage of efferent ducts, epididymal hyperplasia and sterility. *Dev Biol* 2006; 300: 497–511.
35 Evrard YA, Lun Y, Aulehla A, Gan L, Johnson RL. Lunatic fringe is an essential mediator of somite segmentation and patterning. *Nature* 1998; 394: 377–81.
36 Hahn KL, Beres B, Rowton MJ, Skinner MK, Chang Y, *et al.* A deficiency of lunatic fringe is associated with cystic dilation of the rete testis. *Reproduction* 2009; 137: 79–93.
37 Taguchi A, Kaku Y, Ohmori T, Sharmin S, Ogawa M, *et al.* Redefining the *in vivo* origin of metanephric nephron progenitors enables generation of complex kidney structures from pluripotent stem cells. *Cell Stem Cell* 2014; 14: 53–67.
38 Yun K, Ajima R, Sharma N, Costantini F, Mackem S, *et al.* Non-canonical Wnt5a/Ror2 signaling regulates kidney morphogenesis by controlling intermediate mesoderm extension. *Hum Mol Genet* 2014; 23: 6807–14.
39 Jost A. Recherches sur la différenciation sexuelle de l'embryon de Lapin. *Arch Anat Microsc Morphol Exp* 1947; 36: 151–315.
40 Lyon MF, Hawkes SG. X-linked gene for testicular feminization in the mouse. *Nature* 1970; 227: 1217–9.
41 Matsumoto T, Takeyama K, Sato T, Kato S. Androgen receptor functions from reverse genetic models. *J Steroid Biochem Mol Biol* 2003; 85: 95–9.
42 Welsh M, Sharpe RM, Walker M, Smith LB, Saunders PT. New insights into the role of androgens in Wolffian duct stabilization in male and female rodents. *Endocrinology* 2009; 150: 2472–80.
43 Shima Y, Miyabayashi K, Haraguchi S, Arakawa T, Otake H, *et al.* Contribution of Leydig and Sertoli cells to testosterone production in mouse fetal testes. *Mol Endocrinol* 2013; 27: 63–73.
44 DeFalco T, Capel B. Gonad morphogenesis in vertebrates: divergent means to a convergent end. *Annu Rev Cell Dev Biol* 2009; 25: 457–82.
45 Jost A. Problems of fetal endocrinology: the gonadal and hypophyseal hormones. *Recent Prog Horm Res* 1953; 8: 379–418.
46 Renfree MB, Fenelon J, Wijiyanti G, Wilson JD, Shaw G. Wolffian duct differentiation by physiological concentrations of androgen delivered systemically. *Dev Biol* 2009; 334: 429–36.
47 Murashima A, Miyagawa S, Ogino Y, Nishida-Fukuda H, Araki K, *et al.* Essential roles of androgen signaling in Wolffian duct stabilization and epididymal cell differentiation. *Endocrinology* 2011; 152: 1640–51.
48 Cunha GR, Young P, Higgins SJ, Cooke PS. Neonatal seminal vesicle mesenchyme induces a new morphological and functional phenotype in the epithelia of adult ureter and ductus deferens. *Development* 1991; 111: 145–58.
49 Cunha GR, Alarid ET, Turner T, Donjacour AA, Boutin EL, *et al.* Normal and abnormal development of the male urogenital tract. Role of androgens, mesenchymal-epithelial interactions, and growth factors. *J Androl* 1992; 13: 465–75.
50 Donjacour AA, Thomson AA, Cunha GR. FGF-10 plays an essential role in the growth of the fetal prostate. *Dev Biol* 2003; 261: 39–54.
51 Gupta C. The role of epidermal growth factor receptor (EGFR) in male reproductive tract differentiation: stimulation of EGFR expression and inhibition of Wolffian duct differentiation with anti-EGFR antibody. *Endocrinology* 1996; 137: 905–10.
52 Gupta C, Siegel S, Ellis D. The role of EGF in testosterone-induced reproductive tract differentiation. *Dev Biol* 1991; 146: 106–16.
53 Tomaszewski J, Joseph A, Archambeault D, Yao HH. Essential roles of inhibin beta A in mouse epididymal coiling. *Proc Natl Acad Sci U S A* 2007; 104: 11322–7.
54 Nie X, Arend LJ. Pkd1 is required for male reproductive tract development. *Mech Dev* 2013; 130: 567–76.
55 Hirashima T. Pattern formation of an epithelial tubule by mechanical instability during epididymal development. *Cell Rep* 2014; 9: 866–73.
56 Warr N, Siggers P, Bogani D, Brixey R, Pastorelli L, *et al.* Sfrp1 and Sfrp2 are required for normal male sexual development in mice. *Dev Biol* 2009; 326: 273–84.
57 Johnston DS, Jelinsky SA, Bang HJ, DiCandeloro P, Wilson E, *et al.* The mouse epididymal transcriptome: transcriptional profiling of segmental gene expression in the epididymis. *Biol Reprod* 2005; 73: 404–13.
58 Abou-Haïla A, Fain-Maurel MA. Regional differences of the proximal part of mouse epididymis: morphological and histochemical characterization. *Anat Rec* 1984; 209: 197–208.
59 Turner TT, Riley TA. p53 independent, region-specific epithelial apoptosis is induced in the rat epididymis by deprivation of luminal factors. *Mol Reprod Dev* 1999; 53: 188–97.
60 Xu B, Abdel-Fattah R, Yang L, Crenshaw SA, Black MB, *et al.* Testicular lumicrine factors regulate ERK, STAT, and NFKB pathways in the initial segment of the rat epididymis to prevent apoptosis. *Biol Reprod* 2011; 84: 1282–91.
61 Lan ZJ, Labus JC, Hinton BT. Regulation of gamma-glutamyl transpeptidase catalytic activity and protein level in the initial segment of the rat epididymis by testicular factors: role of basic fibroblast growth factor. *Biol Reprod* 1998; 58: 197–206.
62 Kirby JL, Yang L, Labus JC, Hinton BT. Characterization of fibroblast growth factor receptors expressed in principal cells in the initial segment of the rat epididymis. *Biol Reprod* 2003; 68: 2314–21.
63 Sonnenberg E, Gödecke A, Walter B, Bladt F, Birchmeier C. Transient and locally restricted expression of the ros1 protooncogene during mouse development. *EMBO J* 1991; 10: 3693–702.
64 Tessarollo L, Nagarajan L, Parada LF. c-ros: the vertebrate homolog of the sevenless tyrosine kinase receptor is tightly regulated during organogenesis in mouse embryonic development. *Development* 1992; 115: 11–20.
65 Chen J, Zong CS, Wang LH. Tissue and epithelial cell-specific expression of chicken proto-oncogene c-ros in several organs suggests that it may play roles in their development and mature functions. *Oncogene* 1994; 9: 773–80.
66 Keilhack H, Müller M, Böhmer SA, Frank C, Weidner KM, *et al.* Negative regulation of Ros receptor tyrosine kinase signaling. An epithelial function of the SH2 domain protein tyrosine phosphatase SHP-1. *J Cell Biol* 2001; 152: 325–34.
67 Xu B, Yang L, Lye RJ, Hinton BT. p-MAPK1/3 and DUSP6 regulate epididymal cell proliferation and survival in a region-specific manner in mice. *Biol Reprod* 2010; 83: 807–17.
68 Xu B, Yang L, Hinton BT. The role of fibroblast growth factor receptor substrate 2 (FRS2) in the regulation of two activity levels of the components of the extracellular signal-regulated kinase (ERK) pathway in the mouse epididymis. *Biol Reprod* 2013; 89: 1–13.
69 Simanainen U, McNamara K, Davey RA, Zajac JD, Handelsman DJ. Severe subfertility in mice with androgen receptor inactivation in sex accessory organs but not in testis. *Endocrinology* 2008; 149: 3330–8.
70 Krutskikh A, De Gendt K, Sharp V, Verhoeven G, Poutanen M, *et al.* Targeted inactivation of the androgen receptor gene in murine proximal epididymis causes epithelial hypotrophy and obstructive azoospermia. *Endocrinology* 2011; 152: 689–96.
71 O'Hara L, Welsh M, Saunders PT, Smith LB. Androgen receptor expression in the caput epididymal epithelium is essential for development of the initial segment and epididymal spermatozoa transit. *Endocrinology* 2011; 152: 718–29.
72 Sun EL, Flickinger CJ. Development of cell types and of regional differences in the postnatal rat epididymis. *Am J Anat* 1979; 154: 27–55.
73 Da Silva N, Cortez-Retamozo V, Reinecker HC, Wildgruber M, Hill E, *et al.* A dense network of dendritic cells populates the murine epididymis. *Reproduction* 2011; 141: 653–63.
74 Shum WW, Da Silva N, McKee M, Smith PJ, Brown D, *et al.* Transepithelial projections from basal cells are luminal sensors in pseudostratified epithelia. *Cell* 2008; 135: 1108–17.
75 Björkgren I, Saastamoinen L, Krutskikh A, Huhtaniemi I, Poutanen M, *et al.* Dicer1 ablation in the mouse epididymis causes dedifferentiation of the epithelium and imbalance in sex steroid signaling. *PLoS One* 2012; 7: e38457.
76 Ma W, Xie S, Ni M, Huang X, Hu S, *et al.* MicroRNA-29a inhibited epididymal epithelial cell proliferation by targeting nuclear autoantigenic sperm protein (NASP). *J Biol Chem* 2012; 287: 10189–99.
77 Ma W, Hu S, Yao G, Xie S, Ni M, *et al.* An androgen receptor-microrna-29a regulatory circuitry in mouse epididymis. *J Biol Chem* 2013; 288: 29369–81.
78 McGinnis W, Krumlauf R. Homeobox genes and axial patterning. *Cell* 1992; 68: 283–302.
79 Hsieh-Li HM, Witte DP, Weinstein M, Branford W, Li H, *et al.* Hoxa 11 structure, extensive antisense transcription, and function in male and female fertility. *Development* 1995; 121: 1373–85.

[Downloaded free from http://www.ajandrology.com on Tuesday, January 19, 2016, IP: 134.121.42.92]

80 Podlasek CA, Seo RM, Clemens JQ, Ma L, Maas RL, *et al.* Hoxa-10 deficient male mice exhibit abnormal development of the accessory sex organs. *Dev Dyn* 1999; 214: 1–12.
81 Bomgardner D, Hinton BT, Turner TT. Hox transcription factors may play a role in regulating segmental function of the adult epididymis. *J Androl* 2001; 22: 527–31.
82 Snyder EM, Small CL, Bomgardner D, Xu B, Evanoff R, *et al.* Gene expression in the efferent ducts, epididymis, and vas deferens during embryonic development of the mouse. *Dev Dyn* 2010; 239: 2479–91.
83 Jequier AM, Ansell ID, Bullimore NJ. Congenital absence of the vasa deferentia presenting with infertility. *J Androl* 1985; 6: 15–9.
84 Anguiano A, Oates RD, Amos JA, Dean M, Gerrard B, *et al.* Congenital bilateral absence of the vas deferens. A primarily genital form of cystic fibrosis. *JAMA* 1992; 267: 1794–7.
85 Augarten A, Yahav Y, Kerem BS, Halle D, Laufer J, *et al.* Congenital bilateral absence of vas deferens in the absence of cystic fibrosis. *Lancet* 1994; 344: 1473–4.
86 McCallum T, Milunsky J, Munarriz R, Carson R, Sadeghi-Nejad H, *et al.* Unilateral renal agenesis associated with congenital bilateral absence of the vas deferens: phenotypic findings and genetic considerations. *Hum Reprod* 2001; 16: 282–8.
87 Pope JC 4th, Brock JW 3rd, Adams MC, Stephens FD, Ichikawa I. How they begin and how they end: classic and new theories for the development and deterioration of congenital anomalies of the kidney and urinary tract, CAKUT. *J Am Soc Nephrol* 1999; 10: 2018–28.
88 Abdelhak S, Kalatzis V, Heilig R, Compain S, Samson D, *et al.* A human homologue of the *Drosophila* eyes absent gene underlies branchio-oto-renal (BOR) syndrome and identifies a novel gene family. *Nat Genet* 1997; 15: 157–64.
89 Kochhar A, Orten DJ, Sorensen JL, Fischer SM, Cremers CW, *et al.* SIX1 mutation screening in 247 branchio-oto-renal syndrome families: a recurrent missense mutation associated with BOR. *Hum Mutat* 2008; 29: 565.
90 Afzal AR, Rajab A, Fenske CD, Oldridge M, Elanko N, *et al.* Recessive Robinow syndrome, allelic to dominant brachydactyly type B, is caused by mutation of ROR2. *Nat Genet* 2000; 25: 419–22.
91 Person AD, Beiraghi S, Sieben CM, Hermanson S, Neumann AN, *et al.* WNT5A mutations in patients with autosomal dominant Robinow syndrome. *Dev Dyn* 2010; 239: 327–37.
92 Girgis SM, Etriby AN, Ibrahim AA, Kahil SA. Testicular biopsy in azoospermia. A review of the last ten years' experiences of over 800 cases. *Fertil Steril* 1969; 20: 467–77.
93 Kroovand RL, Perlmutter AD. Congenital anomalies of the vas deferens and epididymis. In: SJ Hogan and ESE Hafez, editors. Pediatric Andrology. Boston: Martinus Nijhoff Publishers; 1981. p. 173–80.
94 Turek PJ, Ewalt DH, Snyder HM, Duckett JW. Normal epididymal anatomy in boys. *J Urol* 1994; 151: 726–7.
95 Zvizdic Z, Huskic J, Dizdarevic S, Karavdic K, Zvizdic D. Incidence of epididymal disjunction anomalies associated with an undescended testis. *Folia Med* 2009; 44: 65–8.
96 Tzouanacou E, Wegener A, Wymeersch FJ, Wilson V, Nicolas JF. Redefining the progression of lineage segregations during mammalian embryogenesis by clonal analysis. *Dev Cell* 2009; 17: 365–76.
97 Takemoto T, Uchikawa M, Yoshida M, Bell DM, Lovell-Badge R, *et al.* Tbx6-dependent Sox2 regulation determines neural or mesodermal fate in axial stem cells. *Nature* 2011; 470: 394–8.
98 Chia I, Grote D, Marcotte M, Batourina E, Mendelsohn C, *et al.* Nephric duct insertion is a crucial step in urinary tract maturation that is regulated by a Gata3-Raldh2-Ret molecular network in mice. *Development* 2011; 138: 2089–97.
99 Pole RJ, Qi BQ, Beasley SW. Patterns of apoptosis during degeneration of the pronephros and mesonephros. *J Urol* 2002; 167: 269–71.
100 Wang Q, Lan Y, Cho ES, Maltby KM, Jiang R. Odd-skipped related 1 (Odd 1) is an essential regulator of heart and urogenital development. *Dev Biol* 2005; 288: 582–94.
101 Mattiske D, Kume T, Hogan BL. The mouse forkhead gene Foxc1 is required for primordial germ cell migration and antral follicle development. *Dev Biol* 2006; 290: 447–58.
102 Schuchardt A, D'Agati V, Pachnis V, Costantini F. Renal agenesis and hypodysplasia in ret-k- mutant mice result from defects in ureteric bud development. *Development* 1996; 122: 1919–29.
103 Niederreither K, Subbarayan V, Dollé P, Chambon P. Embryonic retinoic acid synthesis is essential for early mouse post-implantation development. *Nat Genet* 1999; 21: 444–8.
104 Hoshii T, Takeo T, Nakagata N, Takeya M, Araki K, *et al.* LGR4 regulates the postnatal development and integrity of male reproductive tracts in mice. *Biol Reprod* 2007; 76: 303–13.
105 Mendive F, Laurent P, Van Schoore G, Skarnes W, Pochet R, *et al.* Defective postnatal development of the male reproductive tract in LGR4 knockout mice. *Dev Biol* 2006; 290: 421–34.

Developmental Biology 400 (2015) 139–147

Contents lists available at ScienceDirect

Developmental Biology

journal homepage: www.elsevier.com/locate/developmentalbiology

Region-specific regulation of cell proliferation by FGF receptor signaling during the Wolffian duct development

Mika Okazawa [a,b,1], Aki Murashima [a,1], Masayo Harada [c], Naomi Nakagata [d], Masafumi Noguchi [e], Mitsuru Morimoto [e], Tadashi Kimura [b], David M. Ornitz [f], Gen Yamada [a,*]

[a] Department of Developmental Genetics, Institute of Advanced Medicine, Wakayama Medical University, 811-1 Kimiidera, Wakayama 641-8509, Japan
[b] Department of Obstetrics and Gynecology, Osaka University Graduate School of Medicine, 2-2 Yamadaoka, Suita 565-0871, Osaka, Japan
[c] Department of Clinical Anatomy, Graduate School of Medical and Dental Sciences, Tokyo, Medical and Dental University, 1-5-45 Yushima, Bunkyo-ku 113-8519, Tokyo, Japan
[d] Division of Reproductive Engineering, Center for Animal Resources and Development, Kumamoto University, 2-2-1 Honjo, Kumamoto 860-0811, Japan
[e] Laboratory for Lung Development, RIKEN Center for Developmental Biology, 2-2-3 Minatojima-minamimachi, Chuou-ku, Kobe 650-0047, Hyogo, Japan
[f] Department of Developmental Biology, Washington University School of Medicine, St. Louis, MO 63110, USA

ARTICLE INFO

Article history:
Received 22 August 2014
Received in revised form
19 January 2015
Accepted 22 January 2015
Available online 9 February 2015

Keywords:
Fgfr
Ret
Receptor tyrosine kinase
Cell proliferation
Wolffian duct
Ureteric bud

ABSTRACT

The Wolffian duct (WD) is a primordium of the male reproductive tract and kidney collecting duct system. Fibroblast growth factor receptors (FGFRs), members of the receptor tyrosine kinase (RTK) family, are essential for kidney development. Although the functions of FGFR signaling in kidney morphogenesis have been analyzed, their function in WD development has not been comprehensively investigated. Here, we demonstrate that *Fgfr2* is the major *Fgfr* gene expressed throughout the WD epithelia and that it is essential for the maintenance of the WD, specifically in the caudal part of the WD. *Hoxb7-Cre* mediated inactivation of *Fgfr2* in the mouse WD epithelia resulted in the regression of the caudal part of the WD and abnormal male reproductive tract development. Cell proliferation and expression of the downstream target genes of RTK signaling (*Etv4* and *Etv5*) were decreased in the caudal part of the WD epithelia in the mutant embryos. Cranial (rostral) WD formation and ureteric budding were not affected. *Ret*, *Etv4*, and *Etv5* expression were sustained in the ureteric bud of the mutant embryos. Taken together, these data suggest region-specific requirements for FGFR2 signaling in the developing caudal WD epithelia.

© 2015 The Authors. Published by Elsevier Inc. This is an open access article under the CC BY-NC-ND license (http://creativecommons.org/licenses/by-nc-nd/4.0/).

Introduction

The Wolffian duct (WD) is a primordium of the male reproductive tract, which develops into the epididymis, vas deferens, and seminal vesicles. In addition, the WD plays a crucial role in kidney development as the primordium for the ureter and kidney collecting duct system (Bouchard et al., 2002; Saxen, 1987). In mouse embryos, the WD is formed in the anterior intermediate mesoderm at embryonic (E) day 8.5 (E8.5), elongating caudally to reach the cloaca by E9.5 (Atsuta et al., 2013; Davidson, 2009). WD insertion into the cloaca has been reported to be essential for ureter positioning (Chia et al., 2011; Weiss et al., 2014). Three successive kidneys develop along the WD in an anterior–posterior manner: the pronephros, mesonephros, and metanephros (Capel, 2000). The pronephros is formed at the most anterior level of the WD at E8.5, and degenerates by E9.5 (Dressler, 2006). The mesonephros is subsequently formed posterior to the pronephros. The cranial part of the mesonephric mesenchyme differentiates into the mesonephric tubules (MTs) (Dressler, 2006). Degeneration of the mesonephric mesenchyme begins from caudal at E10.5 and extends cranially (Hoshi et al., 2012). At the same time, in the caudal end of the mesonephros, the WD develops a multilayered, "pseudostratified epithelia", forming the ureteric bud (UB) (Chi et al., 2009). The metanephros, which is the definitive kidney in mammals, begins to form from the UB and adjacent metanephric mesenchyme (MM) (Yu et al., 2004). Malformation of the WD in the caudal mesonephros, in addition to the UB, often results in the congenital anomalies in human, such as duplex ureter and absence of the vas deferens. The characterization of the nephrogenic regions, especially the caudal mesonephros, has just started to be understood for their susceptibility to such developmental abnormality (Hoshi et al., 2012; Murashima et al., 2014; Nishita et al., 2014).

* Corresponding author. Fax: +81 73 499 5026.
E-mail addresses: transg8@wakayama-med.ac.jp, genyama77@yahoo.co.jp (G. Yamada).
[1] These authors contributed equally to this work.

http://dx.doi.org/10.1016/j.ydbio.2015.01.023
0012-1606/© 2015 The Authors. Published by Elsevier Inc. This is an open access article under the CC BY-NC-ND license (http://creativecommons.org/licenses/by-nc-nd/4.0/).

The reciprocal interaction between the WD epithelia and adjacent nephrogenic mesenchyme is essential for the morphogenesis of all kidney structures (Batourina et al., 2001). In such interactions, growth factor signaling, including Glial cell line-derived neurotrophic factor (Gdnf), Wnt, and Fibroblast growth factor (Fgf), are well characterized signaling pathways. Dysregulation of these signaling pathways often causes ectopic UB formation, mostly in the caudal part of the mesonephros (Basson et al., 2005; Brophy et al., 2001; Grieshammer et al., 2004; Kume et al., 2000; Mendelsohn, 2009; Michos et al., 2004; Nishita et al., 2014; Shakya et al., 2005).

Receptor tyrosine kinase (RTK) signaling is a key requirement for the development of many organs. It regulates cellular processes including proliferation, survival, differentiation, and migration (Schlessinger, 2000). Binding of ligands to their RTKs activates several intracellular pathways such as phosphoinositide 3-kinase (PI3K)/AKT, mitogen-activated protein kinase (MAPK), and phospholipase C-gamma (PLC-gamma) (Song et al., 2011). Several RTKs such as Rearranged during transfection (RET) and Fgf receptor (FGFR) play an essential role in vertebrae embryonic development, especially in mammalian kidney development (Bates, 2011; Benazeraf and Pourquie, 2013; Costantini and Shakya, 2006; Moore et al., 1996; Pichel et al., 1996; Sainio et al., 1997; Sanchez et al., 1996; Schuchardt et al., 1994).

There are four FGFRs that interact with 18 known FGF ligands in mammals (Beenken and Mohammadi, 2009; Ornitz and Itoh, 2001). The expression of *Fgfr1* and *Fgfr2* is detected in the metanephros and in the cranial part of the mesonephros (Cancilla et al., 1999; Dudley et al., 1999; Kitagaki et al., 2011; Orr-Urtreger et al., 1991; Peters et al., 1992; Poladia et al., 2006; Zhao, 2004). In contrast, *Fgfr3* and *Fgfr4* are not detected in the mesonephros (Kitagaki et al., 2011). Conditional knockout (KO) approaches in mice have revealed that *Fgfr1* and *Fgfr2* in the kidney mesenchyme are crucial for early MM formation and UB induction (Hains et al., 2008; Poladia et al., 2006; Walker et al., 2013). On the other hand, epithelial FGFR signaling regulates the branching morphogenesis of the metanephric kidney, possessing minor functions on initial UB formation (Zhao, 2004). Recent studies indicate that FGFR signaling may compensate loss of GDNF/RET signaling, which is the most essential RTK signaling for the ureteric budding (Maeshima et al., 2007; Michos et al., 2010; Tee et al., 2013). Although the functions of FGF signaling in metanephric kidney morphogenesis have been analyzed, its function in WD development has not been well described. In addition, the possible compensation between different RTKs in the WD has not been investigated.

In this study, we examined the roles of FGFR signaling in the WD using mouse genetic models. WD-specific inactivation of *Fgfr2* revealed a developmental region-specific function for FGFR2 on regulation of cell proliferation.

Materials and methods

Mice

The mouse strains used herein were *Fgfr1*^{flox} (Zhao et al., 2007), *Fgfr2*^{flox} (Yu et al., 2003), *Hoxb7-Cre* (Yu et al., 2002), *ROSA26-LacZ* (Soriano, 1999), *ROSA26-YFP* (Srinivas et al., 2001), *Ret-GFP* (Enomoto et al., 2001) and ICR (CLEA, Tokyo, Japan). *Hoxb7-Cre* mice and *ROSA26-YFP* mice were obtained from Jackson Laboratory. *Fgfr2*-null alleles were generated by crossing *Fgfr2*^{flox} mice to *CAGGS-Cre* mice (Araki et al., 1997), which express Cre recombinase in the germline. All experimental procedures and protocols were approved by the Animal Research Committee of the Wakayama Medical University and Kumamoto University. Embryos for each experiment were collected from at least three pregnant females. Noon on the day when a vaginal plug was detected was designated as E0.5. Embryos used for analyses at E10.5 were not identified their gender. Male embryos were used for the analyses at E12.5 and later.

Histology and immunohistochemistry

Tissues were fixed in 4% paraformaldehyde, dehydrated, embedded in paraffin, and sectioned. Hematoxylin and eosin (HE) staining was performed by standard procedures as previously described (Haraguchi et al., 2000). For immunohistochemistry, deparaffinized sections were treated for antigen retrieval (autoclave 121 °C for 1 min in 10 mM citrate buffer at pH 6.0) and incubated with 3% H_2O_2 in methanol for 10 min to inactivate endogenous peroxidase before 1 h incubation with a blocking solution (1.5% fetal bovine serum (FBS) in PBS). Anti-cleaved caspase-3 polyclonal antibody (Cell Signaling Technology, Danvers, MA, 1:1000), anti-ZO-1 polyclonal antibody (Invitrogen, Carlsbad, CA, 1:200), anti-laminin polyclonal antibody (Sigma-Aldrich, St. Louis, MO, 1:100), or anti-E-cadherin monoclonal antibody (BD Biosciences, San Jose, CA, 1:400) in PBS solution was added to the slides and incubated for 1 h at room temperature. Negative controls were obtained by excluding the primary antibodies. After washing with PBS, the sections were stained with the Vectastain ABC Kit (Vector Laboratories, Burlingame, CA) or incubated with Alexa 546/488-labeled goat anti-rabbit/mouse IgG (Life Technologies, Grand Island, NY) or horseradish peroxidase-labeled rabbit anti-goat IgG (Zymed, South San Francisco, CA) for 1 h at room temperature. Where indicated, the sections were subsequently incubated with 3, 3-diaminobenzidine tetrahydrochloride (DAB) containing H_2O_2. Sections were counterstained by Hoechst 33342 (Sigma-Aldrich), Hematoxylin (Wako, Osaka, Japan), or Methyl Green (Sigma-Aldrich).

Cell proliferation assay

Pregnant females were injected intraperitoneally with 25 mg 5-ethynyl-2′-deoxyuridine (EdU; Invitrogen) per 1 kg body weight. One hour after injection, embryos were collected. Embryos were fixed and processed for paraffin-embedding as described above. Serial horizontal sections (6 μm/section) were made from the cranial end to the caudal end of the WD. EdU-labeled cells were stained using the Click-iT EdU Alexa Fluor 555 Imaging Kit (Invitrogen) according to the supplier's instructions. The total cell number (stained by Hoechst) and the total number of EdU-positive cells were counted for each epithelial portion. The percentage proliferation was calculated as the fraction of EdU-positive cells over the total number of nuclei. Statistical analysis was performed using the Mann–Whitney test ($P < 0.05$ was considered significant).

Whole-mount and section RNA in situ hybridization for gene expression

Whole-mount and section *in situ* hybridization was performed using digoxigenin-labeled probes as previously described (Haraguchi et al., 2000). Probes for the following genes were used: *Pax2* (Dressler et al., 1990), *Fgfr1* (kindly provided by Dr. J. Partanen), *Fgfr2* (Ozawa et al., 1996), *Etv4* (provided by Dr. D. M. Ornitz), *Etv5* (provided by Dr. D. M. Ornitz), *Ret* (Nishinakamura et al., 2001), *Gdnf* (Nishinakamura et al., 2001), and *Fgf10* (kindly provided by Dr. H. Ohuchi and Dr. N. Itoh). For the confirmation of the *Fgfr2* mutation, a probe that does not recognize the mutated allele was used (Yu et al., 2003).

Results

Fgfr2 is the major Fgfr gene expressed in the WD epithelia

Although *Fgfr* expression has been partially reported, their expression in the mesonephros has been poorly described. To identify patterns of *Fgfr* expression in the WD, whole-mount RNA *in situ* hybridization was performed at E10.5. *Fgfr1* and *Fgfr2* were expressed throughout the mesonephros of wild-type embryos at E10.5 (Fig. 1A and E, arrow). *Fgfr1* expression was more prominent in the MTs (Fig. 1A and B, arrowheads) and mesenchyme (Fig. 1B–D) than that in the epithelia of the WD (Fig. 1B–D, dashed line, indicated in Fig. 1I). In contrast, *Fgfr2* expression was more prominent in the epithelia of the WD (Fig. 1F–H, dashed line, indicated in Fig. 1I) compared to the MTs (Fig. 1E and F, arrowheads) and mesenchyme (Fig. 1F–H). *Fgfr2* expression was also observed in the WD epithelia locating near the cloaca (Fig. 1J, dashed line).

WD-specific inactivation of Fgfr2 results in WD regression in the caudal mesonephros

Cre activity driven by the *Hoxb7* promoter was analyzed by crossing *Hoxb7-Cre* mice with the *ROSA26-LacZ* reporter strain and embryos were analyzed for β-galactosidase (βgal) enzyme activity. βgal-positive cells were located throughout the WD epithelia in *Hoxb7-Cre*; $ROSA26^{LacZ/+}$ embryos at E10.5 and E9.5 (Supplemental Fig. S1A–C) (Kobayashi et al., 2005; Mugford et al., 2008; Yu et al., 2002). Most of the epithelial cells were βgal-positive in the WD, and a few βgal-negative cells were observed in the cranial part (Supplemental Fig. S1A, arrow). A small number of βgal-positive cells were observed in MTs (Supplemental Fig. S1A, arrowhead). The percentage of βgal-positive cells in each region of the WD epithelia of *Hoxb7-Cre*; $ROSA26^{LacZ/+}$ embryos at E10.5 was shown in Supplemental Fig. S1 ($n=3$).

To examine the roles of FGFR2 signaling during WD development, *Hoxb7-Cre*; $Fgfr2^{+/-}$ male mice were crossed with $Fgfr1^{flox/flox}$; $Fgfr2^{flox/flox}$ female mice to get *Hoxb7-Cre*; $Fgfr1^{flox/+}$; $Fgfr2^{flox/-}$ embryos. Hereafter, we refer to *Hoxb7-Cre*; $Fgfr1^{flox/+}$; $Fgfr2^{flox/-}$ mice as WD-specific *Fgfr2*-inactivation mice ($Fgfr2^{WD\ flox/-}$). Control mice are either heterozygous for the *Fgfr2* floxed allele (*Hoxb7-Cre*; $Fgfr1^{flox/+}$; $Fgfr2^{flox/+}$) or lack the *Hoxb7-Cre* transgenic allele.

Inactivation of *Fgfr2* in the WD of $Fgfr2^{WD\ flox/-}$ embryos was confirmed by whole-mount RNA *in situ* hybridization. *Fgfr2* was expressed in the WD and MTs in the control embryos at E10.5, while its expression was reduced in $Fgfr2^{WD\ flox/-}$ embryos compared to the controls at E10.5 (Fig. 2A and A′, black arrow and arrowheads). To examine the development of WD structure in $Fgfr2^{WD\ flox/-}$ mice, whole-mount RNA *in situ* hybridization for *Pax2* was performed. *Pax2* expression was observed in the WD, MTs, and condensed mesenchyme in both control and $Fgfr2^{WD\ flox/-}$ embryos at E10.5 (Fig. 2B and B′, black arrow, black arrowheads, and white arrowheads). The MTs were formed along the cranial WD (Fig. 2B and B′, black arrowheads) and the UB invaginated dorsally (Fig. 2B and B′, yellow arrow), showing no significant differences between the control and $Fgfr2^{WD\ flox/-}$ embryos. Histological analysis showed a well-established epithelial structure in the cranial part of the WD in both control and $Fgfr2^{WD\ flox/-}$ embryos at E10.5 (Fig. 2E and E′, black arrow, indicated in Fig. 2S). In the caudal part, no significant differences were observed in the size of the WD between the control and some $Fgfr2^{WD\ flox/-}$ embryos (3 out of total 7 samples), whereas a hypoplastic WD of the caudal mesonephros was observed in other $Fgfr2^{WD\ flox/-}$ embryos (4 out of total 7 samples; Fig. 2F and F′, black arrow, also indicated in Fig. 2S). The ductal epithelia reached the cloacal epithelia in both control and $Fgfr2^{WD\ flox/-}$ embryos at E10.5 (7 out of total 7 samples; Fig. 2L and L′, black arrowheads). The well-differentiated pseudostratified epithelia of the UB were detected even in $Fgfr2^{WD\ flox/-}$ embryos with hypoplastic WD of the caudal mesonephros (Fig. 2G and G′, also indicated in Fig. 2S). These data indicate that the WD is formed in the mutant embryos by E10.5. At E12.5, the WD marked by *Pax2* expression was observed from cranial to caudal of the control embryos (Fig. 2C). In contrast, such *Pax2* expression was disrupted in the WD of the caudal mesonephros of $Fgfr2^{WD\ flox/-}$ embryos (Fig. 2C′, red arrow). Histological analysis revealed that the cranial epithelial structure was indistinguishable between the control and $Fgfr2^{WD\ flox/-}$ WD (Fig. 2H and H′, indicated in Fig. 2T). In contrast, the WD of the caudal mesonephros showed regressing epithelia in $Fgfr2^{WD\ flox/-}$ embryos (a red arrow in

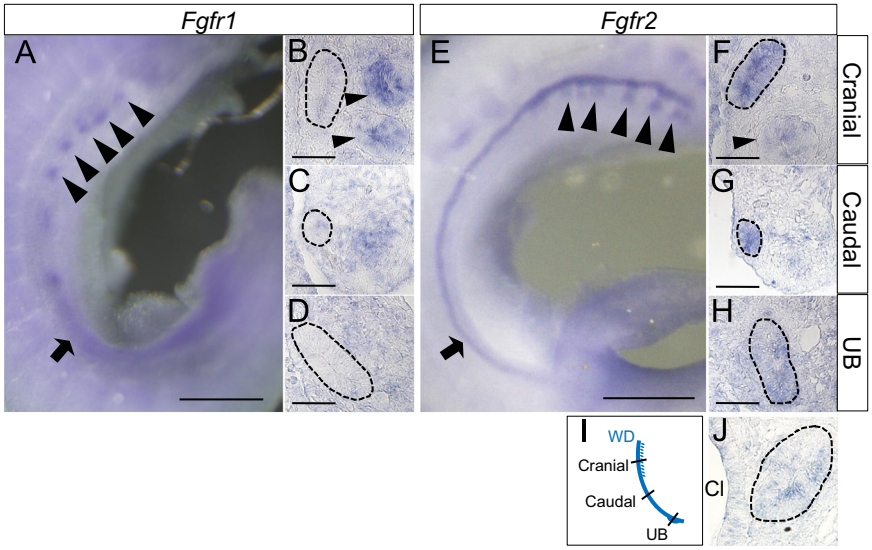

Fig. 1. *Fgfr2* is the major *Fgfr* gene expressed in the WD epithelia. Whole-mount RNA *in situ* hybridization to detect *Fgfr1* (A) and *Fgfr2* (E) expression in the mesonephros of wild-type embryos was performed at E10.5. Section RNA *in situ* hybridization to detect *Fgfr1* (B–D) and *Fgfr2* (F–H, and J) expression in the mesonephros of wild-type embryos was performed at E10.5. For the histological analyses of horizontal sections at E10.5, the WD is divided into three parts along the axis by the following definition: (1) cranial part, the WD where MTs are present; (2) caudal part, the WD of the caudal mesonephros (the WD between the cranial part and the UB); and (3) UB part, the WD where the pseudostratified epithelia is observed. A schematic representation of the cranial (B and F), caudal (C and G), and UB (D and H) parts in the WD at E10.5 are presented in I. *Fgfr2* expression in the portion that lies near the cloaca is shown in J. Scale bars: A and E, 500 μm; B–D, F–H, and J, 50 μm. Arrow, WD; arrowheads, MTs; dashed line, WD epithelia; Cl, cloaca.

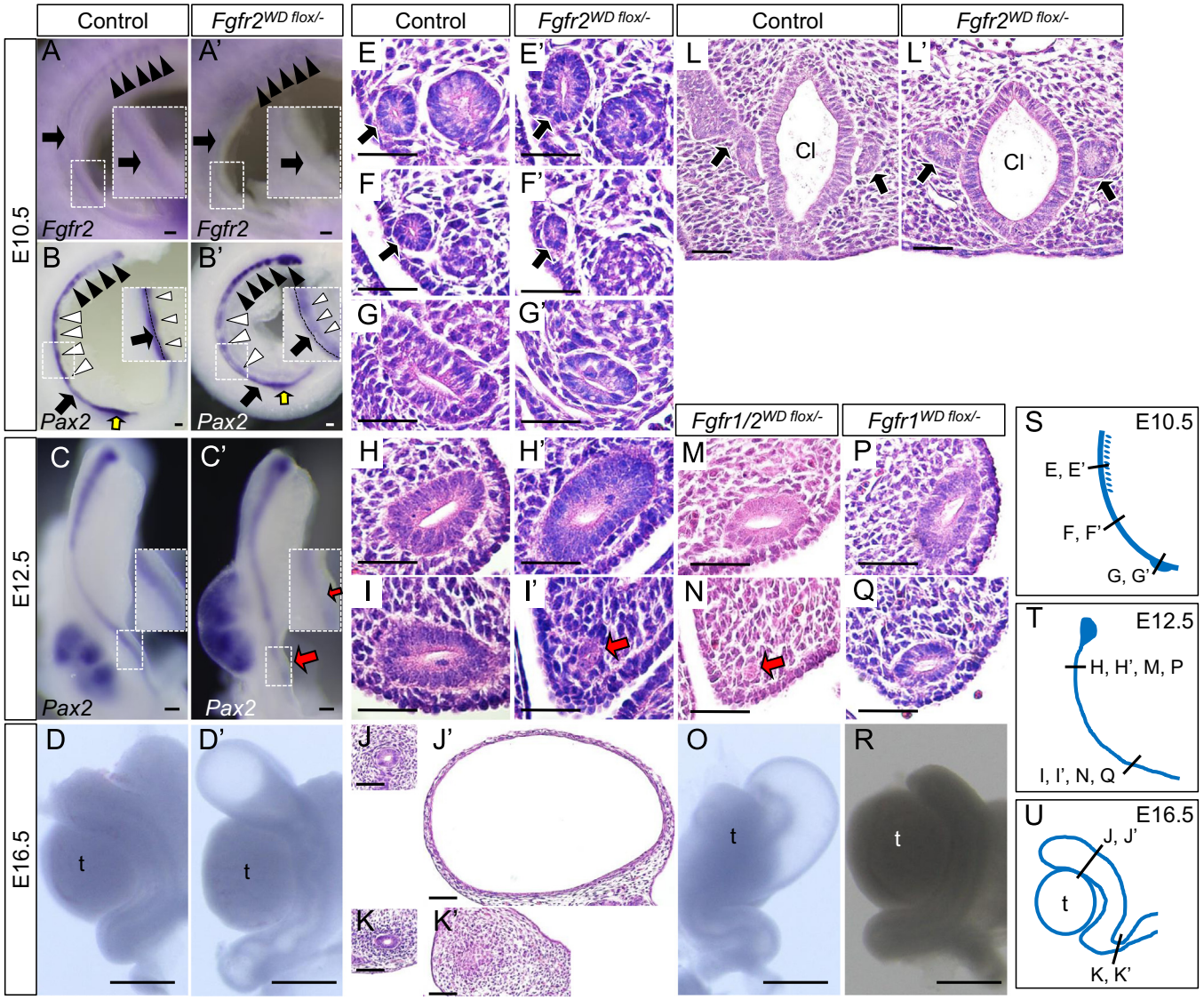

Fig. 2. WD-specific inactivation of *Fgfr2* results in WD regression in the caudal mesonephros. Whole-mount RNA *in situ* hybridization to detect *Fgfr2* expression in the WD and MTs of the control (A) and $Fgfr2^{WD\ flox/-}$ (A′) embryos was performed at E10.5. Insets show high magnification views of the caudal mesonephros (A and A′). The WD and MTs are marked by *Pax2* expression in the control (B and C) and $Fgfr2^{WD\ flox/-}$ (B′ and C′) embryos at E10.5 (B and B′) and E12.5 (C and C′). Insets show high magnification views of the caudal mesonephros (B, B′, C and C′). The gross morphology of the WD and testis at E16.5 is shown in D (control) and D′ ($Fgfr2^{WD\ flox/-}$). HE staining of the WD in the control (E–L) and $Fgfr2^{WD\ flox/-}$ (E′–L′) embryos was performed at E10.5 (E–G, L, E′–G′, and L′), E12.5 (H, I, H′, and I′), and E16.5 (J, K, J′, and K′). Schematic representations indicating the axial levels of the WD at E10.5, E12.5, and E16.5 are presented in S, T, and U. The WD that lies near the cloaca is shown in L (Control) and L′ ($Fgfr2^{WD\ flox/-}$). HE staining at E12.5 and the gross morphology of the WD and testis at E16.5 in $Fgfr1/2^{WD\ flox/-}$ and $Fgfr1^{WD\ flox/-}$ embryos are shown in M–O and P–R. Scale bars: A–C and A′–C′, 100 μm; D, D′, O, and R, 500 μm; E–N, P, Q, and E′–L′, 50 μm. Black arrow, WD; black arrowheads, MTs; white arrowheads, condensed mesenchyme; yellow arrow, UB; red arrow, regression of WD epithelia; Cl, cloaca; t, testis.

Fig. 2I′, also indicated in Fig. 2T; 8 out of total 10 samples in Table 1). Taken together, these results suggest that epithelial FGFR signaling is essential for the maintenance of the WD, especially in the caudal mesonephros. At E16.5, the control embryos possessed well-differentiated WD derivatives, the epididymis and vas deferens, connected to the urogenital sinus (Fig. 2D). $Fgfr2^{WD\ flox/-}$ embryos, on the other hand, showed a dilation of the duct in the cranial WD (Fig. 2D, D′, J, and J′, indicated in Fig. 2U; 4 out of total 6 samples in Table 1), and the epithelial structure was not observed in the vas deferens derived from the WD of the caudal mesonephros (Fig. 2K and K′, also indicated in Fig. 2U).

Functional redundancy of *Fgfr1* and *Fgfr2* has been reported in several developmental systems (Hebert, 2003; Paek et al., 2009; White et al., 2006). To examine the function of *Fgfr1* upon inactivation of *Fgfr2* in the WD epithelia, *Hoxb7-Cre*; $Fgfr1^{flox/-}$; $Fgfr2^{flox/-}$ ($Fgfr1/2^{WD\ flox/-}$) mice were investigated. $Fgfr1/2^{WD\ flox/-}$ embryos showed regressing epithelia in the WD of the caudal mesonephros at E12.5 (Fig. 2N, red arrow; 3 out of total 3 samples in Table 1), as observed in $Fgfr2^{WD\ flox/-}$ embryos (Fig. 2I′; 8 out of total 10 samples in Table 1). In contrast, the epithelial structure was indistinguishable in the cranial part between the control and $Fgfr1/2^{WD\ flox/-}$ WDs (Fig. 2H and M). At E16.5, the gross morphology of $Fgfr1/2^{WD\ flox/-}$ embryos showed dilated duct formation in the cranial part, with an obstructed duct in the caudal part at E16.5 (Fig. 2O; 2 out of total

Table 1
Phenotypic incidence of $Fgfr2^{WD\ flox/-}$, $Fgfr1/2^{WD\ flox/-}$ and $Fgfr1^{WD\ flox/-}$ embryos.

Individual allele with genotype	E12.5	E16.5
Hoxb7-Cre; $Fgfr1^{flox/+}$; $Fgfr2^{flox/-}$ ($Fgfr2^{WD\ flox/-}$)	8/10	4/6
Hoxb7-Cre; $Fgfr1^{flox/-}$; $Fgfr2^{flox/-}$ ($Fgfr1/2^{WD\ flox/-}$)	3/3	2/3
Hoxb7-Cre; $Fgfr1^{flox/-}$; $Fgfr2^{flox/+}$ ($Fgfr1^{WD\ flox/-}$)	0/8	0/4

3 samples in Table 1), as observed in *Fgfr2*$^{WD\ flox/-}$ embryos (Fig. 2D′; 4 out of total 6 samples in Table 1). By the histological analysis of the *Fgfr1/2*$^{WD\ flox/-}$ WD, the presence of epithelia in the cranial part was observed, while the epithelial structure was not evident in the caudal part (data not shown), as observed in *Fgfr2*$^{WD\ flox/-}$ embryos (Fig. 2J′ and K′). *Hoxb7-Cre*; *Fgfr1*$^{flox/-}$; *Fgfr2*$^{flox/+}$ (*Fgfr1*$^{WD\ flox/-}$) embryos showed no obvious phenotypes; well-differentiated WDs reached the urogenital sinus as well as the control WD at E16.5 (Fig. 2R, $n=4$ in Table 1) and at E12.5 (Fig. 2P and Q; $n=8$ in Table 1). This is consistent with the absence of prominent *Fgfr1* expression in the WD epithelia during WD development (Fig. 1B–D). These results indicate that *Fgfr2* is the dominant FGF receptor for the maintenance of the WD in the caudal mesonephros, and *Fgfr1* may contribute with a small amount of redundancy.

Decreased expression of the downstream target genes of RTK signaling in the WD epithelia of Fgfr2$^{WD\ flox/-}$ *embryos*

Etv4 and *Etv5* are downstream targets of RTK signaling including FGFR (Brent and Tabin, 2004; Firnberg and Neubüser, 2002; Liu et al., 2003). The expression pattern of *Etv4* and *Etv5* in the WD was examined at the WD of the cranial and caudal mesonephros, and UB (Fig. 3N). Both *Etv4* and *Etv5* were expressed in the WD epithelia, MT, and condensed nephrogenic mesenchyme of E10.5 control embryos (dashed line, black arrowhead, and white arrowhead in Fig. 3A–C and D–F). Expression of these genes was reduced in the WD epithelia of the cranial and caudal mesonephros of *Fgfr2*$^{WD\ flox/-}$ embryos, compared to control embryos (Fig. 3A, A′, B, B′, D, D′, E and E′, dashed line). The expression of these genes was not significantly different in the MTs (Fig. 3A, A′, D, and D′, black arrowhead) and the condensed mesenchyme (Fig. 3B, B′, E, and E′, white arrowhead) between the control and *Fgfr2*$^{WD\ flox/-}$ embryos. Notably, the expression of *Etv4* and *Etv5* in the epithelia adjacent to the MM (MM side) was retained at the UB level, whereas it was decreased in the epithelia at the opposite side of the MM (coelom side) in *Fgfr2*$^{WD\ flox/-}$ embryos (Fig. 3C, C′, F, and F′, red arrowheads, indicated in Fig. 3O).

In addition to FGFR signaling, GDNF/RET signaling is also essential RTK signaling for UB formation (Cacalano et al., 1998; Enomoto et al., 1998; Moore et al., 1996; Pichel et al., 1996; Sanchez et al., 1996; Schuchardt et al., 1994). Failure of UB formation is the most frequent phenotype associated with *Gdnf* or *Ret* deficiency (Costantini and Shakya, 2006). In control embryos, *Ret* was expressed throughout the WD epithelia (Fig. 3G–I, dashed line; Fig. 3J, black arrow), with the highest level of expression in the UB at E10.5 (Fig. 3I, dashed line; Fig. 3J, yellow arrow). In contrast, *Ret* expression was reduced in the WD of the cranial and caudal mesonephros, and in the coelom side of the UB of *Fgfr2*$^{WD\ flox/-}$ embryos (Fig. 3G–I and G′–H′, dashed line, red arrowheads; Fig. 3J and J′, black arrow). *Ret* expression in the MM side of the UB was not affected in *Fgfr2*$^{WD\ flox/-}$ embryos at E10.5 (Fig. 3I′, dashed line; Fig. 3J′, yellow arrow). These results suggest that *Ret* expression may be regulated by *Fgfr2* in the WD epithelia, except in the MM side of the UB. This observation is consistent with the finding that UB outgrowth was unaffected in *Fgfr2*$^{WD\ flox/-}$ embryos until E13.5 (data not shown) (Zhao, 2004).

In the WD, it is reported that chimeric expression of *Ret* in the UB results in epithelial cell rearrangement to exclude the *Ret*-negative cells from the MM side of the UB (Chi et al., 2009). To trace the lineage of cells in which Cre was activated in the *Fgfr2*$^{WD\ flox/-}$ background, we crossed *Hoxb7-Cre*; *Fgfr2*$^{+/-}$ mice with *Fgfr2*$^{flox/flox}$; *ROSA26*$^{YFP/YFP}$ mice to obtain *Hoxb7-Cre*; *ROSA26*$^{YFP/+}$; *Fgfr2*$^{flox/-}$

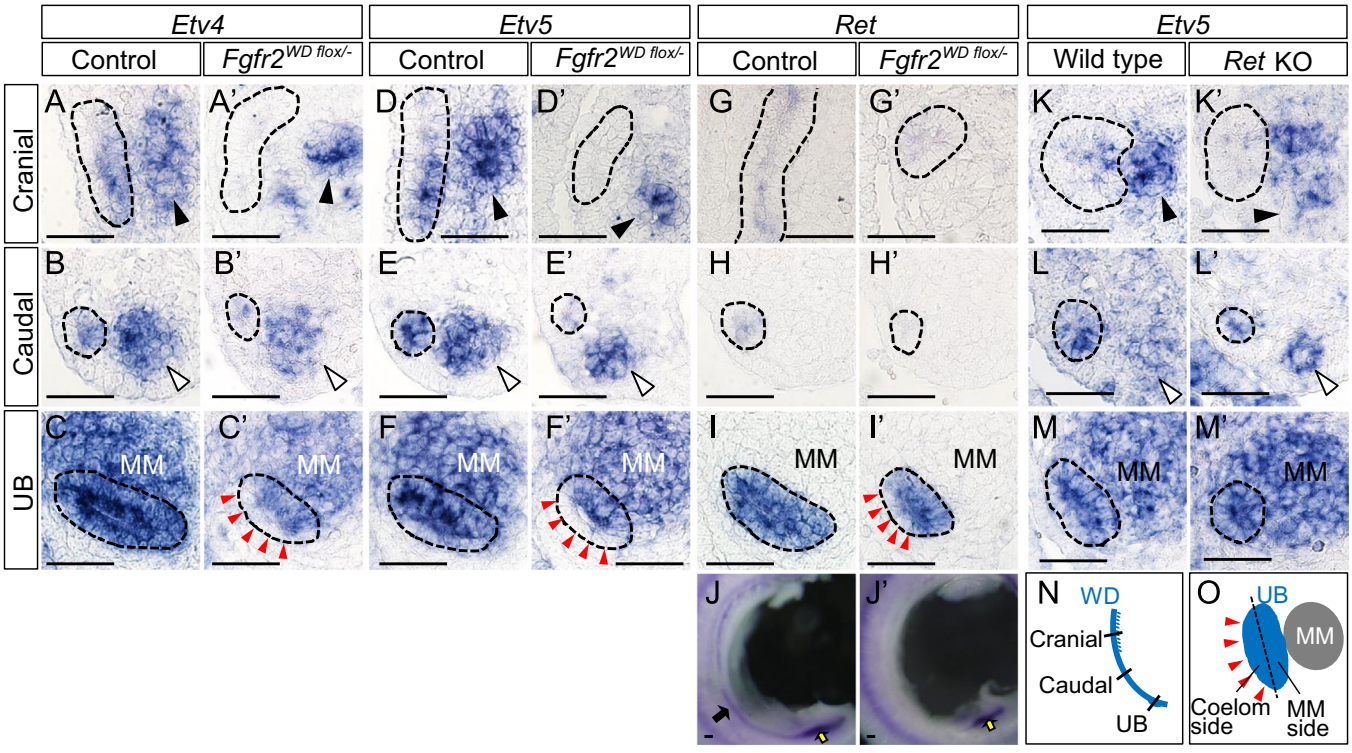

Fig. 3. Decreased expression of the downstream target genes of RTK signaling in the WD epithelia of *Fgfr2*$^{WD\ flox/-}$ embryos. Section RNA *in situ* hybridization for *Etv4* (A–C and A′–C′), *Etv5* (D–F and D′–F′), and *Ret* (G–I and G′–I′) in E10.5 embryos in the cranial (A, A′, D, D′, G, and G′), caudal (B, B′, E, E′, H, and H′), and UB (C, C′, F, F′, I, and I′) parts was performed in the control (A–I) and *Fgfr2*$^{WD\ flox/-}$ (A′–I′) embryos. Whole-mount RNA *in situ* hybridization to detect *Ret* expression was performed in the control (J) and *Fgfr2*$^{WD\ flox/-}$ (J′) embryos at E10.5. Section RNA *in situ* hybridization for *Etv5* in wild-type (K–M) and *Ret* KO (K′–M′) embryos for the cranial (K and K′), caudal (L and L′), and UB (M and M′) parts was performed at E10.5. A schematic representation of the cranial, caudal, and UB parts in the WD at E10.5 is shown in N. A schematic representation of the MM and coelom sides of the UB at E10.5 is shown in O. Scale bars: A–I, K–M, A′–I′, and K′–M′, 50 μm; J and J′, 100 μm. Dashed line, WD epithelia; black arrowhead, MT; white arrowhead, condensed mesenchyme; MM, metanephric mesenchyme; red arrows, coelom side of the UB; yellow arrow, UB.

embryos. Recombined cells, marked by GFP, were distributed throughout the WD and displayed no significant differences when compared with *Hoxb7-Cre*; *ROSA26*$^{LacZ/+}$ embryos at E10.5 (Supplemental Figs. S1 and S2). Uniform distribution of the recombined cells in the UB was observed in *Fgfr2*$^{WD\ flox/-}$ embryos (Supplemental Fig. S2). These results suggest that *Hoxb7-Cre*-mediated *Fgfr2* gene recombination in the WD was introduced ubiquitously and recombined cell-specific epithelial cell rearrangement may not occur in the *Fgfr2*$^{WD\ flox/-}$ WDs. Taken together, these results suggest that FGFR2 signaling is the major RTK signaling pathway in the WD epithelia, but not in the MM side of the UB, at E10.5.

To examine the involvement of GDNF/RET signaling in *Etv* expression in the WD, we analyzed *Ret* KO mice at E10.5. *Ret* gene mutations lead to renal agenesis and hypoplasia, and ectopic ureter termination (de Graaff et al., 2001; Enomoto et al., 2001; Jain et al., 2006; Schuchardt et al., 1996). Sustained expression of *Etv4* and *Etv5* was observed in all regions of the WD epithelia of *Ret* KO embryos (dashed line in Fig. 3K–M and K′–M′, data not shown). However, reduced phospho-Erk expression was observed in the MM side of the UB of *Ret* KO embryos at E10.5 (data not shown), which agrees with the previous finding (Chi et al., 2009). These results suggest that the reduced expression of *Etv4* and *Etv5* observed in *Fgfr2*$^{WD\ flox/-}$ embryos is independent of RET-mediated RTK signaling.

FGFR signaling regulates cell proliferation in the WD of the caudal mesonephros and the coelom side of the UB

To identify the mechanism leading to the regression of the WD of the caudal mesonephros in *Fgfr2*$^{WD\ flox/-}$ embryos, cell proliferation was assessed by EdU incorporation at the WD of the cranial and caudal mesonephros, and UB at E10.5 (Fig. 4A–C and A′–C′; indicated in Fig. 4N). In control embryos, the WD of the caudal mesonephros and the UB displayed higher rate of cell proliferation than the cranial part (Fig. 4A–C). The WD of the caudal mesonephros in the *Fgfr2*$^{WD\ flox/-}$ embryos demonstrated significantly reduced epithelial cell proliferation, compared to the control embryos (Fig. 4B, B′, and M). There were no significant differences in cell proliferation in the cranial part and in the MM side of the UB between the control and *Fgfr2*$^{WD\ flox/-}$ WDs (Fig. 4A, A′, C, C′ and M). Fewer proliferating cell nuclei were observed in the coelom side of the UB in *Fgfr2*$^{WD\ flox/-}$ embryos than in the control embryos (Fig. 4C, C′, and M). Apoptosis, indicated by cleaved caspase-3 expression, was also analyzed in control and *Fgfr2*$^{WD\ flox/-}$ embryos. No significant differences in apoptosis were observed between the control and *Fgfr2*$^{WD\ flox/-}$ embryos at E10.5 (Fig. 4D–F and D′–F′, red arrowheads). These results indicate that FGFR signaling regulates cell proliferation in the WD of the caudal mesonephros and in the coelom side of the UB.

To investigate whether loss of epithelial cell polarity contributes to the epithelial regression observed in *Fgfr2*$^{WD\ flox/-}$ WDs, expression patterns of ZO-1 (Fig. 4G–I and G′–I′), E-cadherin, and laminin (Fig. 4J–L and J′–L′) was analyzed. The core tight junction protein, ZO-1, was detected at the apical side of epithelial cells in both control and *Fgfr2*$^{WD\ flox/-}$ WDs (Fig. 4G–I and G′–I′). E-cadherin, an adherence junction protein, and laminin, a basement membrane component, were detected at the apical and lateral side of the cells and at the basement membrane, respectively, in *Fgfr2*$^{WD\ flox/-}$ WDs as well as in control embryos (Fig. 4J–L and J′–L′). These results suggest that polarized epithelia are established and maintained in *Fgfr2*$^{WD\ flox/-}$ WDs.

Region-specific expression of RTK ligands in the mesonephros and metanephros

FGF7 and FGF10 are ligands with high specificity for the FGFR2-IIIb isoform (Ornitz et al., 1996; Zhang et al., 2006). Previous studies have demonstrated that *Fgf7* is not detected in the developing kidney before E14.5 (Finch et al., 1995; Mason et al., 1994). On the other hand, FGF10 is considered the main ligand for FGFR in the WD (Donjacour et al., 2003).

Fgf10 expression was observed in both the MM and the mesenchyme of the coelom side with a pattern showing a higher expression at the UB level that gradually decreases as it proceeds cranially (Fig. 5A and B, Supplemental Fig. S4). *Gdnf*, a ligand for RET signaling, was expressed mainly in the MM of the control embryos (Fig. 5C and D). Localization of *Fgf10* and *Gdnf* expression in the *Fgfr2*$^{WD\ flox/-}$ embryos was essentially similar to that in the control embryos (Fig. 5A–D and A′–D′).

Discussion

WD as a model for ductal formation and its abnormalities

The current study demonstrates that FGFR2 signaling prevents WD regression in the caudal mesonephros, and that loss of FGFR2 in the WD may lead to dilation of the cranial part of the WD. A previous study using FGF10 null mice reported cystic dilation in the epididymis and degeneration of the vas deferens (Donjacour et al., 2003). However, the corresponding mechanisms were not identified. In the current study, we demonstrated that reduced FGF signaling in the WD epithelia results in WD regression in the caudal mesonephros. Luminal fluid from the testis to the WD is essential for further development of the WD into male reproductive tract (Hinton et al., 2000; Shum et al., 2011; Tong et al., 1996). Since fluid secretion commences at approximately E13–14 in mice (Joseph et al., 2009), the obstruction of the WD in the caudal mesonephros in *Fgfr2*$^{WD\ flox/-}$ embryos may cause accumulation of the fluid, leading to dilation of the cranial part of the WD at E16.5.

Formation of the common nephric duct (CND), the WD which locates caudally to the UB, was observed in both the control and *Fgfr2*$^{WD\ flox/-}$ embryos at E12.5 (Supplemental Fig. S3A and A′). At E14.5, the CND was eliminated, and the WD and ureter were separated in the control and *Fgfr2*$^{WD\ flox/-}$ embryos (Supplemental Fig. S3B, B′, C, and C′; the level of B and B′ is more anterior than that of C and C′). Our observation that the WD and the ureter were inserted into the urogenital sinus separately at E14.5 suggests that the dilation of the cranial epididymal duct was a consequence of the obstruction of the duct, not of back-flow of urine. Another potential mechanism underlying such dilation might be the disruption of oriented cell division, as described previously in the kidney of *Fgfr1* and *Fgfr2* double mutant mice (Sims-Lucas et al., 2012).

The WD also grows craniocaudally after reaching the cloaca. Immunohistochemical analysis for ZO-1, E-cadherin, and laminin expressions indicated that the epithelial cells maintained their characteristics in *Fgfr2*$^{WD\ flox/-}$ WDs at E10.5. Cell proliferation is considered to be the major contributor for WD elongation, and the WD of the caudal mesonephros is the most mitotically active in the WD (Fig. 4A–C) (Dyche, 1979; Joseph et al., 2009; Michael and Davies, 2004). Considering that apoptosis was not increased in *Fgfr2*$^{WD\ flox/-}$ WDs compared to control WDs at E10.5, it is possible that decreased cell proliferation in the WD of the caudal mesonephros causes the ductal thinning observed in *Fgfr2*$^{WD\ flox/-}$ embryos at E12.5 and later. The current study suggests that active cell proliferation regulated by FGFR signaling in the WD of the caudal mesonephros is essential to maintain the ductal size and epithelial integrity in the growing duct at a later stage.

RTK signaling via FGFR is required for WD development

The current study demonstrates that WD epithelial cell proliferation is regulated by distinct region-specific FGFR signaling.

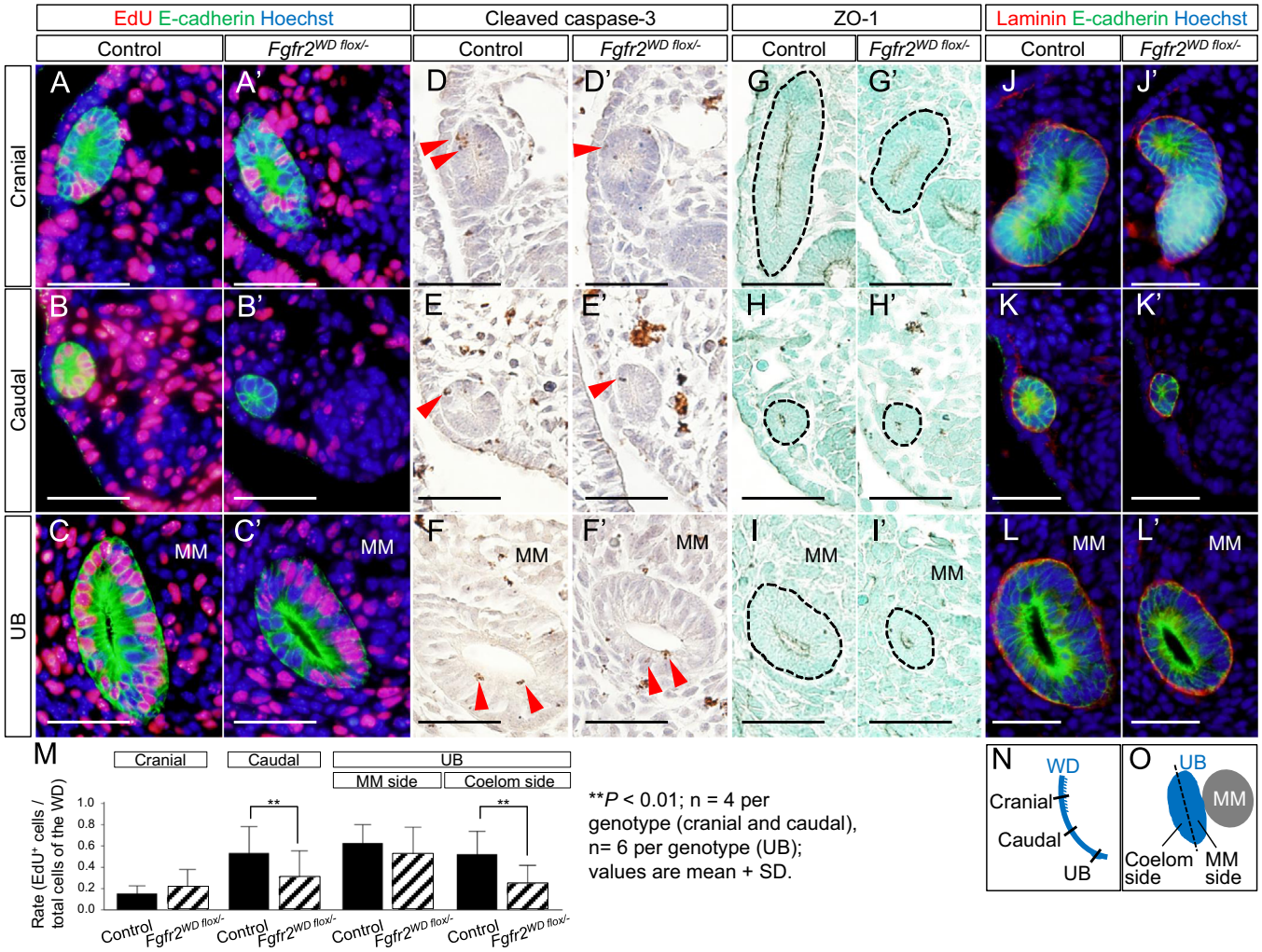

Fig. 4. FGFR signaling regulates cell proliferation in the WD of the caudal mesonephros and the coelom side of the UB. Proliferative cells were labeled with EdU (red) and co-stained with E-cadherin (green) at the cranial (A and A′), caudal (B and B′), and UB (C and C′) parts in the control (A–C) and *Fgfr2*$^{WD\ flox/-}$ (A′–C′) embryos. Nuclei were stained with Hoechst 33342. Immunohistochemistry for cleaved caspase-3 demonstrated the presence of apoptotic cells at the axial levels of the cranial (D and D′), caudal (E and E′), and UB (F and F′) parts in the control (D–F) and *Fgfr2*$^{WD\ flox/-}$ embryos (D′–F′). Sections were counterstained with hematoxylin. Immunohistochemistry for ZO-1 was performed at the axial levels of the cranial (G and G′), caudal (H and H′), and UB (I and I′) parts in the control (G–I) and *Fgfr2*$^{WD\ flox/-}$ (G′–I′) embryos. Sections were counterstained with methyl green. Immunofluorescence staining of laminin (red) and E-cadherin (green) in sections of E10.5 WD was performed at the axial levels of the cranial (J and J′), caudal (K and K′), and UB (L and L′) parts in the control (J–L) and *Fgfr2*$^{WD\ flox/-}$ (J′–L′) embryos. Nuclei were stained with Hoechst 33342. The graph (M) demonstrated the rate of EdU-positive cells per total cells in the WD epithelia in the control and *Fgfr2*$^{WD\ flox/-}$ embryos. A schematic representation of the cranial, caudal, and UB parts in the WD at E10.5 is presented in N. The UB is divided into two domains, the MM side and coelom side, as indicated in O. Scale bars: 50 μm. Red arrowheads, signals of cleaved caspase-3; dashed line, WD epithelia; MM, metanephric mesenchyme.

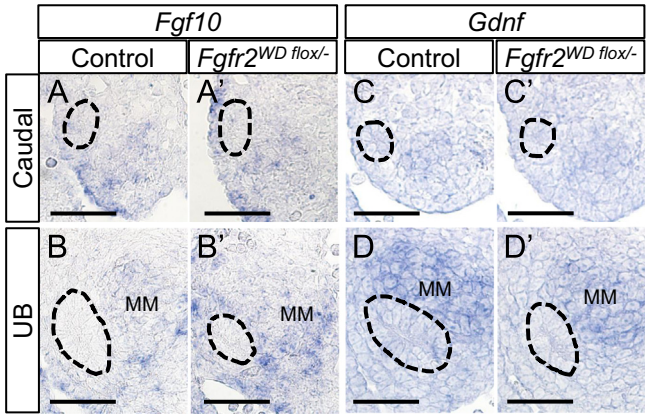

Fig. 5. Region-specific distribution of RTK ligands in the mesonephros and metanephros. Section RNA *in situ* hybridization for *Fgf10* (A, A′, B, and B′) and *Gdnf* (C, C′, D, and D′) in the caudal mesonephros (A, A′, C, and C′) and UB (B, B′, D, and D′) was performed in the control (A–D) and *Fgfr2*$^{WD\ flox/-}$ (A′–D′) embryos at E10.5. Scale bars: 50 μm. Dashed line, WD epithelia; MM, metanephric mesenchyme.

The frequency of βgal-negative cells in the cranial WD epithelia of *Hoxb7-Cre*; *ROSA26*$^{LacZ/+}$ embryos was higher than that in the WD of the caudal mesonephros and UB. It is possible that the sustained epithelial cell proliferation in the cranial part of mutant WDs might be due to lower activity of *Hoxb7-Cre* in the cranial WD epithelia. However, significant reduction of active RTK signaling, indicated by *Etv4* and *Etv5* expression, was observed in the cranial part of *Fgfr2*$^{WD\ flox/-}$ WDs compared to control WDs. These results suggest that RTK signaling is sufficiently reduced in the cranial part of *Fgfr2*$^{WD\ flox/-}$ WDs. Taken together, RTK signaling through *Etv4* and *Etv5* may possess less contribution to epithelial cell proliferation in the cranial WD. *Fgf8* is expressed in MTs at E10.5 and its mesoderm-specific conditional KO mice display degeneration in the cranial part of the WD and missing cranial MTs (Kitagaki et al., 2011). Moreover, mesoderm-specific conditional KO mice for *Fgfr1* and *Fgfr2* show loss of the WD and MTs (Kitagaki et al., 2011). These observations may suggest that FGFR signaling in MTs or in the nephrogenic mesenchyme is essential for the maintenance of the cranial part of the WD.

In *Fgfr2*$^{WD\ flox/-}$ embryos, epithelial cell proliferation in the MM side of the UB did not show any significant reduction. The expression pattern of *Ret*, *Etv4*, and *Etv5* in *Fgfr2*$^{WD\ flox/-}$ embryos indicated that RTK signaling via RET was retained in the MM side of the UB. These results are consistent with the previous findings that UB outgrowth is regulated mainly by GDNF/RET signaling (Moore et al., 1996; Pichel et al., 1996; Sainio et al., 1997; Sanchez et al., 1996; Schuchardt et al., 1994). In *Ret* KO mice, almost 40% of embryos show ureteric budding, and additional inhibition of FGFR signaling completely abolishes UB formation (Michos et al., 2010; Schuchardt et al., 1994). These previous observations indicate partial redundancy between RET and FGFR signaling in the UB.

The current work demonstrated that *Ret* expression was reduced in the WD epithelia, except in the MM side of the UB in *Fgfr2*$^{WD\ flox/-}$ embryos, suggesting that *Fgfr2* probably regulates GDNF/RET signaling in the WD of the caudal mesonephros and the coelom side of the UB. However, analysis of *Ret* KO embryos suggests that GDNF/RET signaling is dispensable for *Etv* expression and also for cell proliferation (data not shown) in these parts. These results indicate that RTK signaling via FGFR is required for WD development.

To our knowledge, *Fgf10* is the only RTK ligand that is distinctly expressed in the mesenchyme of the caudal mesonephros and of the coelom side of the UB at E10.5. In contrast, *Gdnf* is prominently expressed in the metanephric mesenchyme. This region-specific expression pattern of RTK ligands may explain the region-specific FGFR2 dependency of RTK signaling in the WD epithelia, *i.e.*, the possible redundancy of RTK signaling between FGF and GDNF in the MM side of the UB but not in the coelom side and the WD of the caudal mesonephros.

In conclusion, the current study demonstrates that WD epithelial cell proliferation is regulated by distinct region-specific mechanisms during its development. The results suggest that FGFR signaling is essential for cell proliferation of the WD in the caudal mesonephros and the coelom side of the UB. The WD is fundamental not only for the development of the transient or definitive kidneys but also for the development of the reproductive tract. The WD is also essential for the formation of the Mullerian duct (MD), female reproductive tract anlarge. The MD extends from cranial to caudal under the guidance of the WD around E12.5 (Mullen and Behringer, 2014). Therefore, it is possible that the abnormality observed in the current mutant embryos may also consequently affect the MD development and female reproductive tract development. Further analyses regarding female embryos may provide broad function of FGF signaling in reproductive tract formation. The current study provides novel insights into the regulation of urogenital tract development, including male and female reproductive tract, and kidney.

Acknowledgments

We thank Dr. Hideki Enomoto, Dr. Anne M. Moon, Dr. Chuxia Deng, Dr. Ryuichi Nishinakamura, Dr. Nobuyuki Itoh, and Dr. Hideyo Ohuchi for their supports. We also express our appreciation to Dr. Kentaro Suzuki, Dr. Daisuke Matsumaru, Dr. Akiko Omori, Dr. Lerrie A. Ipulan, Dr. Dennis D. Raga, Hiroko Suzuki, Shoko Matsushita, and Yoshitsugu Sakita for their assistance. We thank Tomiko I. Iba for technical help. This work is supported by Grant-in-Aid for Young Scientists B (25860771) and for Scientific Research on Innovative Areas: Molecular mechanisms for establishment of Sex differences (22132006). This work is also supported by National Institutes of Health Grant R01ES016597 (G. Yamada) and R01HL111190 (D. M. Ornitz).

Appendix A. Supporting information

Supplementary data associated with this article can be found in the online version at http://dx.doi.org/10.1016/j.ydbio.2015.01.023.

References

Araki, K., Imaizumi, T., Okuyama, K., Oike, Y., Yamamura, K., 1997. Efficiency of recombination by Cre transient expression in embryonic stem cells: comparison of various promoters. J. Biochem. 122, 977–982.
Atsuta, Y., Tadokoro, R., Saito, D., Takahashi, Y., 2013. Transgenesis of the Wolffian duct visualizes dynamic behavior of cells undergoing tubulogenesis *in vivo*. Dev. Growth Differ. 55, 579–590.
Basson, M.A., Akbulut, S., Watson-Johnson, J., Simon, R., Carroll, T.J., Shakya, R., Gross, I., Martin, G.R., Lufkin, T., McMahon, A.P., Wilson, P.D., Costantini, F.D., Mason, I.J., Licht, J.D., 2005. Sprouty1 is a critical regulator of GDNF/RET-mediated kidney induction. Dev. Cell 8, 229–239.
Bates, C.M., 2011. Role of fibroblast growth factor receptor signaling in kidney development. Am. J. Physiol. Renal Physiol. 301, F245–251.
Batourina, E., Gim, S., Bello, N., Shy, M., Clagett-Dame, M., Srinivas, S., Costantini, F., Mendelsohn, C., 2001. Vitamin A controls epithelial/mesenchymal interactions through Ret expression. Nat. Genet. 27, 74–78.
Beenken, A., Mohammadi, M., 2009. The FGF family: biology, pathophysiology and therapy. Nat. Rev. Drug Discov. 8, 235–253.
Benazeraf, B., Pourquie, O., 2013. Formation and segmentation of the vertebrate body axis. Annu. Rev. Cell Dev. Biol. 29, 1–26.
Bouchard, M., Souabni, A., Mandler, M., Neubuser, A., Busslinger, M., 2002. Nephric lineage specification by Pax2 and Pax8. Genes Dev. 16, 2958–2970.
Brent, A.E., Tabin, C.J., 2004. FGF acts directly on the somitic tendon progenitors through the Ets transcription factors Pea3 and Erm to regulate scleraxis expression. Development 131, 3885–3896.
Brophy, P.D., Ostrom, L., Lang, K.M., Dressler, G.R., 2001. Regulation of ureteric bud outgrowth by Pax2-dependent activation of the glial derived neurotrophic factor gene. Development 128, 4747–4756.
Cacalano, G., Farinas, I., Wang, L.C., Hagler, K., Forgie, A., Moore, M., Armanini, M., Phillips, H., Ryan, A.M., Reichardt, L.F., Hynes, M., Davies, A., Rosenthal, A., 1998. GFRalpha1 is an essential receptor component for GDNF in the developing nervous system and kidney. Neuron 21, 53–62.
Cancilla, B., Ford-Perriss, M.D., Bertram, J.F., 1999. Expression and localization of fibroblast growth factors and fibroblast growth factor receptors in the developing rat kidney. Kidney Int. 56, 2025–2039.
Capel, B., 2000. The battle of the sexes. Mech. Dev. 92, 89–103.
Chi, X., Michos, O., Shakya, R., Riccio, P., Enomoto, H., Licht, J.D., Asai, N., Takahashi, M., Ohgami, N., Kato, M., Mendelsohn, C., Costantini, F., 2009. Ret-dependent cell rearrangements in the Wolffian duct epithelium initiate ureteric bud morphogenesis. Dev. Cell 17, 199–209.
Chia, I., Grote, D., Marcotte, M., Batourina, E., Mendelsohn, C., Bouchard, M., 2011. Nephric duct insertion is a crucial step in urinary tract maturation that is regulated by a Gata3–Raldh2–Ret molecular network in mice. Development 138, 2089–2097.
Costantini, F., Shakya, R., 2006. GDNF/Ret signaling and the development of the kidney. BioEssays: News Rev. Mol. Cell. Dev. Biol. 28, 117–127.
Davidson, A., 2009. Mouse Kidney Development. StemBook.
de Graaff, E., Srinivas, S., Kilkenny, C., D'Agati, V., Mankoo, B.S., Costantini, F., Pachnis, V., 2001. Differential activities of the RET tyrosine kinase receptor isoforms during mammalian embryogenesis. Genes Dev. 15, 2433–2444.
Donjacour, A.A., Thomson, A.A., Cunha, G.R., 2003. FGF-10 plays an essential role in the growth of the fetal prostate. Dev. Biol. 261, 39–54.
Dressler, G.R., 2006. The cellular basis of kidney development. Annu. Rev. Cell Dev. Biol. 22, 509–529.
Dressler, G.R., Deutsch, U., Chowdhury, K., Nornes, H.O., Gruss, P., 1990. Pax2, a new murine paired-box-containing gene and its expression in the developing excretory system. Development 109, 787–795.
Dudley, A.T., Godin, R.E., Robertson, E.J., 1999. Interaction between FGF and BMP signaling pathways regulates development of metanephric mesenchyme. Genes Dev. 13, 1601–1613.
Dyche, W.J., 1979. A comparative study of the differentiation and involution of the Mullerian duct and Wolffian duct in the male and female fetal mouse. J. Morphol. 162, 175–209.
Enomoto, H., Araki, T., Jackman, A., Heuckeroth, R.O., Snider, W.D., Johnson Jr., E.M., Milbrandt, J., 1998. GFR alpha1-deficient mice have deficits in the enteric nervous system and kidneys. Neuron 21, 317–324.
Enomoto, H., Crawford, P.A., Gorodinsky, A., Heuckeroth, R.O., Johnson Jr., E.M., Milbrandt, J., 2001. RET signaling is essential for migration, axonal growth and axon guidance of developing sympathetic neurons. Development 128, 3963–3974.
Finch, P.W., Cunha, G.R., Rubin, J.S., Wong, J., Ron, D., 1995. Pattern of keratinocyte growth factor and keratinocyte growth factor receptor expression during mouse fetal development suggests a role in mediating morphogenetic mesenchymal–epithelial interactions. Dev. Dyn. Off. Publ. Am. Assoc. Anat. 203, 223–240.

Firnberg, N., Neubüser, A., 2002. FGF signaling regulates expression of Tbx2, Erm, Pea3, and Pax3 in the early nasal region. Dev. Biol. 247, 237–250.
Grieshammer, U., Le, M., Plump, A.S., Wang, F., Tessier-Lavigne, M., Martin, G.R., 2004. SLIT2-mediated ROBO2 signaling restricts kidney induction to a single site. Dev. Cell 6, 709–717.
Hains, D., Sims-Lucas, S., Kish, K., Saha, M., McHugh, K., Bates, C.M., 2008. Role of fibroblast growth factor receptor 2 in kidney mesenchyme. Pediatr. Res. 64, 592–598.
Haraguchi, R., Suzuki, K., Murakami, R., Sakai, M., Kamikawa, M., Kengaku, M., Sekine, K., Kawano, H., Kato, S., Ueno, N., Yamada, G., 2000. Molecular analysis of external genitalia formation: the role of fibroblast growth factor (Fgf) genes during genital tubercle formation. Development 127, 2471–2479.
Hebert, J.M., 2003. FGF signaling through FGFR1 is required for olfactory bulb morphogenesis. Development 130, 1101–1111.
Hinton, B.T., Lan, Z.J., Lye, R.J., Labus, J.C., 2000. Regulation of epididymal function by testicular factors: the lumicrine hypothesis. In: Goldberg, E. (Ed.), The Testis. Springer, New York, pp. 163–173.
Hoshi, M., Batourina, E., Mendelsohn, C., Jain, S., 2012. Novel mechanisms of early upper and lower urinary tract patterning regulated by RetY1015 docking tyrosine in mice. Development 139, 2405–2415.
Jain, S., Encinas, M., Johnson Jr., E.M., Milbrandt, J., 2006. Critical and distinct roles for key RET tyrosine docking sites in renal development. Genes Dev. 20, 321–333.
Joseph, A., Yao, H., Hinton, B.T., 2009. Development and morphogenesis of the Wolffian/epididymal duct, more twists and turns. Dev. Biol. 325, 6–14.
Kitagaki, J., Ueda, Y., Chi, X., Sharma, N., Elder, C.M., Truffer, E., Costantini, F., Lewandoski, M., Perantoni, A.O., 2011. FGF8 is essential for formation of the ductal system in the male reproductive tract. Development 138, 5369–5378.
Kobayashi, A., Kwan, K.M., Carroll, T.J., McMahon, A.P., Mendelsohn, C.L., Behringer, R.R., 2005. Distinct and sequential tissue-specific activities of the LIM-class homeobox gene Lim1 for tubular morphogenesis during kidney development. Development 132, 2809–2823.
Kume, T., Deng, K., Hogan, B.L., 2000. Murine forkhead/winged helix genes Foxc1 (Mf1) and Foxc2 (Mfh1) are required for the early organogenesis of the kidney and urinary tract. Development 127, 1387–1395.
Liu, Y., Jiang, H., Crawford, H.C., Hogan, B.L.M., 2003. Role for ETS domain transcription factors Pea3/Erm in mouse lung development. Dev. Biol. 261, 10–24.
Maeshima, A., Sakurai, H., Choi, Y., Kitamura, S., Vaughn, D.A., Tee, J.B., Nigam, S.K., 2007. Glial cell-derived neurotrophic factor independent ureteric bud outgrowth from the Wolffian duct. J. Am. Soc. Nephrol.: JASN 18, 3147–3155.
Mason, I.J., Fuller-Pace, F., Smith, R., Dickson, C., 1994. FGF-7 (keratinocyte growth factor) expression during mouse development suggests roles in myogenesis, forebrain regionalisation and epithelial-mesenchymal interactions. Mech. Dev. 45, 15–30.
Mendelsohn, C., 2009. Using mouse models to understand normal and abnormal urogenital tract development. Organogenesis 5, 306–314.
Michael, L., Davies, J.A., 2004. Pattern and regulation of cell proliferation during murine ureteric bud development. J. Anat. 204, 241–255.
Michos, O., Cebrian, C., Hyink, D., Grieshammer, U., Williams, L., D'Agati, V., Licht, J.D., Martin, G.R., Costantini, F., 2010. Kidney development in the absence of Gdnf and Spry1 requires Fgf10. PLoS Genet. 6, e1000809.
Michos, O., Panman, L., Vintersten, K., Beier, K., Zeller, R., Zuniga, A., 2004. Gremlin-mediated BMP antagonism induces the epithelial–mesenchymal feedback signaling controlling metanephric kidney and limb organogenesis. Development 131, 3401–3410.
Moore, M.W., Klein, R.D., Farinas, I., Sauer, H., Armanini, M., Phillips, H., Reichardt, L.F., Ryan, A.M., Carver-Moore, K., Rosenthal, A., 1996. Renal and neuronal abnormalities in mice lacking GDNF. Nature 382, 76–79.
Mugford, J.W., Sipila, P., McMahon, J.A., McMahon, A.P., 2008. Osr1 expression demarcates a multi-potent population of intermediate mesoderm that undergoes progressive restriction to an Osr1-dependent nephron progenitor compartment within the mammalian kidney. Dev. Biol. 324, 88–98.
Mullen, R.D., Behringer, R.R., 2014. Molecular genetics of Mullerian duct formation, regression and differentiation. Sex. Dev. Genet. Mol. Biol. Evol. Endocrinol. Embryol. Pathol. Sex Determ. Differ. 8, 281–296.
Murashima, A., Akita, H., Okazawa, M., Kishigami, S., Nakagata, N., Nishinakamura, R., Yamada, G., 2014. Midline-derived Shh regulates mesonephric tubule formation through the paraxial mesoderm. Dev. Biol. 386, 216–226.
Nishinakamura, R., Matsumoto, Y., Nakao, K., Nakamura, K., Sato, A., Copeland, N.G., Gilbert, D.J., Jenkins, N.A., Scully, S., Lacey, D.L., Katsuki, M., Asashima, M., Yokota, T., 2001. Murine homolog of SALL1 is essential for ureteric bud invasion in kidney development. Development 128, 3105–3115.
Nishita, M., Qiao, S., Miyamoto, M., Okinaka, Y., Yamada, M., Hashimoto, R., Iijima, K., Otani, H., Hartmann, C., Nishinakamura, R., Minami, Y., 2014. Role of Wnt5a-Ror2 signaling in morphogenesis of the metanephric mesenchyme during ureteric budding. Mol. Cell Biol. 34, 3096–3105.
Ornitz, D.M., Itoh, N., 2001. Fibroblast growth factors. Genome Biol. 2 (REVIEWS3005).
Ornitz, D.M., Xu, J., Colvin, J.S., McEwen, D.G., MacArthur, C.A., Coulier, F., Gao, G., Goldfarb, M., 1996. Receptor specificity of the fibroblast growth factor family. J. Biol. Chem. 271, 15292–15297.
Orr-Urtreger, A., Givol, D., Yayon, A., Yarden, Y., Lonai, P., 1991. Developmental expression of two murine fibroblast growth factor receptors, flg and bek. Development 113, 1419–1434.
Ozawa, K., Uruno, T., Miyakawa, K., Seo, M., Imamura, T., 1996. Expression of the fibroblast growth factor family and their receptor family genes during mouse brain development. Brain Res. Mol. Brain Res. 41, 279–288.
Paek, H., Gutin, G., Hebert, J.M., 2009. FGF signaling is strictly required to maintain early telencephalic precursor cell survival. Development 136, 2457–2465.
Peters, K.G., Werner, S., Chen, G., Williams, L.T., 1992. Two FGF receptor genes are differentially expressed in epithelial and mesenchymal tissues during limb formation and organogenesis in the mouse. Development 114, 233–243.
Pichel, J.G., Shen, L., Sheng, H.Z., Granholm, A.C., Drago, J., Grinberg, A., Lee, E.J., Huang, S.P., Saarma, M., Hoffer, B.J., Sariola, H., Westphal, H., 1996. Defects in enteric innervation and kidney development in mice lacking GDNF. Nature 382, 73–76.
Poladia, D.P., Kish, K., Kutay, B., Hains, D., Kegg, H., Zhao, H., Bates, C.M., 2006. Role of fibroblast growth factor receptors 1 and 2 in the metanephric mesenchyme. Dev. Biol. 291, 325–339.
Sainio, K., Suvanto, P., Davies, J., Wartiovaara, J., Wartiovaara, K., Saarma, M., Arumae, U., Meng, X., Lindahl, M., Pachnis, V., Sariola, H., 1997. Glial-cell-line-derived neurotrophic factor is required for bud initiation from ureteric epithelium. Development 124, 4077–4087.
Sanchez, M.P., Silos-Santiago, I., Frisen, J., He, B., Lira, S.A., Barbacid, M., 1996. Renal agenesis and the absence of enteric neurons in mice lacking GDNF. Nature 382, 70–73.
Saxen, L., 1987. Organogenesis of the Kidney. Cambridge University Press, New York, USA.
Schlessinger, J., 2000. Cell signaling by receptor tyrosine kinases. Cell 103, 211–225.
Schuchardt, A., D'Agati, V., Larsson-Blomberg, L., Costantini, F., Pachnis, V., 1994. Defects in the kidney and enteric nervous system of mice lacking the tyrosine kinase receptor Ret. Nature 367, 380–383.
Schuchardt, A., D'Agati, V., Pachnis, V., Costantini, F., 1996. Renal agenesis and hypodysplasia in ret-k- mutant mice result from defects in ureteric bud development. Development 122, 1919–1929.
Shakya, R., Jho, E.H., Kotka, P., Wu, Z., Kholodilov, N., Burke, R., D'Agati, V., Costantini, F., 2005. The role of GDNF in patterning the excretory system. Dev. Biol. 283, 70–84.
Shum, W.W., Ruan, Y.C., Da Silva, N., Breton, S., 2011. Establishment of cell–cell cross talk in the epididymis: control of luminal acidification. J. Androl. 32, 576–586.
Sims-Lucas, S., Di Giovanni, V., Schaefer, C., Cusack, B., Eswarakumar, V.P., Bates, C.M., 2012. Ureteric morphogenesis requires Fgfr1 and Fgfr2/Frs2alpha signaling in the metanephric mesenchyme. J. Am. Soc. Nephrol. 23, 607–617.
Song, R., El-Dahr, S.S., Yosypiv, I.V., 2011. Receptor tyrosine kinases in kidney development. J. Signal Transduct. 2011, 869281.
Soriano, P., 1999. Generalized lacZ expression with the ROSA26 Cre reporter strain. Nat. Genet. 21, 70–71.
Srinivas, S., Watanabe, T., Lin, C.S., William, C.M., Tanabe, Y., Jessell, T.M., Costantini, F., 2001. Cre reporter strains produced by targeted insertion of EYFP and ECFP into the ROSA26 locus. BMC Dev. Biol. 1, 4.
Tee, J.B., Choi, Y., Dnyanmote, A., Decambre, M., Ito, C., Bush, K.T., Nigam, S.K., 2013. GDNF-independent ureteric budding: role of PI3K-independent activation of AKT and FOSB/JUN/AP-1 signaling. Biol. Open 2, 952–959.
Tong, S.Y., Hutson, J.M., Watts, L.M., 1996. Does testosterone diffuse down the wolffian duct during sexual differentiation? J. Urol. 155, 2057–2059.
Walker, K.A., Sims-Lucas, S., Di Giovanni, V.E., Schaefer, C., Sunseri, W.M., Novitskaya, T., de Caestecker, M.P., Chen, F., Bates, C.M., 2013. Deletion of fibroblast growth factor receptor 2 from the peri-Wolffian duct stroma leads to ureteric induction abnormalities and vesicoureteral reflux. PloS One 8, e56062.
Weiss, A.C., Airik, R., Bohnenpoll, T., Greulich, F., Foik, A., Trowe, M.O., Rudat, C., Costantini, F., Adams, R.H., Kispert, A., 2014. Nephric duct insertion requires EphA4/EphA7 signaling from the pericloacal mesenchyme. Development 141, 3420–3430.
White, A.C., Xu, J., Yin, Y., Smith, C., Schmid, G., Ornitz, D.M., 2006. FGF9 and SHH signaling coordinate lung growth and development through regulation of distinct mesenchymal domains. Development 133, 1507–1517.
Yu, J., Carroll, T.J., McMahon, A.P., 2002. Sonic hedgehog regulates proliferation and differentiation of mesenchymal cells in the mouse metanephric kidney. Development 129, 5301–5312.
Yu, J., McMahon, A.P., Valerius, M.T., 2004. Recent genetic studies of mouse kidney development. Curr. Opin. Genet. Dev. 14, 550–557.
Yu, K., Xu, J., Liu, Z., Sosic, D., Shao, J., Olson, E.N., Towler, D.A., Ornitz, D.M., 2003. Conditional inactivation of FGF receptor 2 reveals an essential role for FGF signaling in the regulation of osteoblast function and bone growth. Development 130, 3063–3074.
Zhang, X., Ibrahimi, O.A., Olsen, S.K., Umemori, H., Mohammadi, M., Ornitz, D.M., 2006. Receptor specificity of the fibroblast growth factor family. The complete mammalian FGF family. J. Biol. Chem. 281, 15694–15700.
Zhao, H., 2004. Role of fibroblast growth factor receptors 1 and 2 in the ureteric bud. Dev. Biol. 276, 403.
Zhao, M., Li, D., Shimazu, K., Zhou, Y.X., Lu, B., Deng, C.X., 2007. Fibroblast growth factor receptor-1 is required for long-term potentiation, memory consolidation, and neurogenesis. Biol. Psychiatry 62, 381–390.

Original Article

Sexual Development

Sex Dev 2017;11:190–202
DOI: 10.1159/000477452

Accepted: March 28, 2017
by M. Schmid
Published online: July 27, 2017

Androgen Regulates Dimorphic F-Actin Assemblies in the Genital Organogenesis

Liqing Liu[a, b] Kentaro Suzuki[c] Eunice Chun[d] Aki Murashima[c, e] Yuki Sato[f] Naomi Nakagata[g] Toshihiko Fujimori[h] Shigenobu Yonemura[i] Wanzhong He[b] Gen Yamada[c]

[a]National Laboratory of Biomacromolecules, Institute of Biophysics, Chinese Academy of Sciences and [b]National Institute of Biological Sciences, Beijing, China; [c]Department of Developmental Genetics, Wakayama Medical University, Wakayama, Japan; [d]PIC Philippines, Inc., Pasig City, Philippines; [e]Division of Human Embryology, Department of Anatomy, Iwate Medical University, Nishitokuta Yahaba; [f]Department of Anatomy and Cell Biology, Kyushu University Graduate School of Medicine, Fukuoka, [g]Division of Reproductive Engineering, Center for Animal Resources and Development, Kumamoto University, Kumamoto, [h]Division of Embryology, National Institute for Basic Biology, Okazaki, and [i]Department of Cell Biology, Tokushima University Graduate School of Medical Science, Tokushima, Japan

Keywords
Cell migration · Extracellular matrix · F-actin · Masculinization programming window · Urethral mesenchymal cells

Abstract
Impaired androgen activity induces defective sexual differentiation of the male reproductive tract, including hypospadias, an abnormal formation of the penile urethra. Androgen signaling in the urethral mesenchyme cells (UMCs) plays essential roles in driving dimorphic urethral development. However, cellular events for sexual differentiation remain virtually unknown. In this study, histological analyses, fluorescent staining, and transmission electron microscopy (TEM) were performed to reveal the cellular dimorphisms of UMCs. F-actin dynamics and migratory behaviors of UMCs were further analyzed by time-lapse imaging. We observed a prominent accumulation of F-actin with poorly assembled extracellular matrix (ECM) in female UMCs. In contrast, thin fibrils of F-actin co-aligning with the ECM through membrane receptors were identified in male UMCs. Processes for dimorphic F-actin assemblies were temporally identified during an androgen-regulated masculinization programming window and spatially distributed in several embryonic reproductive tissues. Stage-dependent modulation of the F-actin sexual patterns by androgen in UMCs was also demonstrated by time-lapse analysis. Moreover, androgen regulates coordinated migration of UMCs. These results suggest that androgen signaling regulates the assembly of F-actin from cytoplasmic accumulation to membranous fibrils. Such alteration appears to promote the ECM assembly and the mobility of UMCs, contributing to male type genital organogenesis.

© 2017 S. Karger AG, Basel

The reproductive organs possess the sexually specific structures to perform the reproductive function. External genitalia are one of the representative organs showing the sexual differences, with the penile urethra being responsible for copulation and urination in the male. The genital tubercle (GT) is the common anlage for the external genitalia of both the male and the female. Androgen regulates masculinization processes of the male reproductive organs contributing to the dimorphic development of the GT. 5α-dihydrotestosterone (DHT) is the

KARGER

© 2017 S. Karger AG, Basel

E-Mail karger@karger.com
www.karger.com/sxd

Kentaro Suzuki or Gen Yamada
Department of Developmental Genetics, Wakayama Medical University
Kimiidera 811-1,Wakayama City
Wakayama 641-8509 (Japan)
E-Mail k-suzuki@wakayama-med.ac.jp or gensan7@wakayama-med.ac.jp

Downloaded by:
Washington State Univ Lib
134.121.42.92 - 12/20/2017 6:03:57 PM

major androgen for GT masculinization. Testosterone (T) is converted into DHT in the ventral GT mesenchyme by the local 5α-reductase [Suzuki et al., 2017]. Mesenchymally-derived androgen signaling is indispensable for the formation of the penile urethra [Miyagawa et al., 2009]. Genetic and molecular mechanisms involved in androgen driven formation of the penile urethra have been studied [Yong et al., 2007; Miyagawa et al., 2009; Chen et al., 2010]. However, the mode of androgen actions regulating cellular differentiation of urethral mesenchymal cells (UMCs) in ventral GT remains to be elucidated.

Androgen actions are required in a specific time window, namely the masculinization programming window (MPW), to regulate multiple processes for the formation of male-type reproductive organs [Welsh et al., 2008, 2014]. Impaired activities of androgen actions within the MPW induce defective male sexual differentiation, such as hypospadias, prostate hypoplasia, and a shorter anogenital distance [Welsh et al., 2008; Suzuki et al., 2015]. Hypospadias is an ectopic opening of the penile urethra in the ventral external genitalia. The incidence of hypospadias ranges from 1:200~1:300 in male newborns [Manson and Carr, 2003; Cunha et al., 2015] and has been reported as increasing over the past few decades due to environmental exposure of anti-androgenic endocrine disruptors [Wilhelm and Koopman, 2006; Cunha et al., 2015]. The critical time window for urethral masculinization is from embryonic day 15.5 (E15.5) to E16.5 in mice [Miyagawa et al., 2009]. Improper exposure of androgen within the time window causes the several degrees of hypospadias. It remains largely unknown how androgen play roles in the differentiation of UMCs within the MPW.

Cytoskeletons regulate cell morphology and cell movement [Alberts, 2008; Heisenberg and Bellaiche, 2013]. The dynamics of actin assembly provide a mechanical basis for cellular behaviors, such as cell mobility and assembly of the extracellular matrix (ECM) [Blanchoin et al., 2014]. Cultured fibroblast cells have been one of the popular models to study cell biology in vitro [Grinnell, 2008; Friedl and Wolf, 2010; Luo et al., 2013]. However, how the assembling pattern of F-actin contributes to the function of mesenchymal fibroblasts during developmental processes remains poorly understood.

In the current study, we observed dynamic sexually different patterns of F-actin in UMCs during urethral formation. Such sexual patterns were regulated by androgen within the MPW. Furthermore, formation of dimorphic F-actin patterns was spatial-temporally consistent with the embryonic sexual differentiation processes of several reproductive organs. Of note, dimorphic assemblies of F-actin may correlate with the sexual differences of both ECM assemblies and migratory behaviors of UMCs. These results suggest that sexually different assemblies of F-actin may contribute to dimorphic reproductive organogenesis.

Materials and Methods

Animals

Mice expressing Actin-Venus (CDB0253K) and Lyn-Venus [Abe et al., 2011] under the control of the Rosa26 Loci were used for time-lapse imaging analysis of tissue slices. $AR^{Flox/Flox}$ [Sato et al., 2004] females were mated with CAG-Cre [Araki et al., 1997] males to obtain *AR* knockout males (AR^{Flox}/y: CAG^{Cre}, hereafter designated as ARKO males) [Murashima et al., 2011].

Histology

Hematoxylin and Eosin (H & E) and Masson Trichrome staining were performed by standard procedures as previously described [Ogi et al., 2005; Haraguchi et al., 2007]. Tissue sections were prepared into 6 μm in thickness for H & E staining and 4 μm for Masson's Trichrome staining.

F-Actin and Immuno-Fluorescent Staining for Confocal Microscopy

GT and other embryonic tissues at various stages were fixed in 1% PFA at 4°C for 1 h and rinsed and embedded in Cryomold (Tissue-TEK, Sakura, 4566) with OCT compound (Tissue-TEK, Sakura, 4583). Samples were frozen and stored at –80°C. Cryosections were dissected into 12 μm thickness by a freezing microtome (Leica CM1900), mounted on poly-lysin coated slides, dried briefly for 0.5 h at room temperature (RT), and were re-fixed with 1% PFA on ice for 20 min before staining. F-actin was stained with Alexa-488/647 phalloidin (Invitrogen) following the manufacturer's protocol. In the experiments of F-actin co-staining with other antibodies, phalloidin staining was performed during the secondary antibody incubation. Samples were dissected and fixed with 4% PFA at 37°C for α-tubulin staining. Antibodies for α-tubulin (Abcam, Ab52866; 1:300), vimentin (Sigma, V6630; 1:500), fibronectin (Sigma, F1141; 1:500), integrin α5 (BD Pharmingen, 553318; 1:500), and non-muscle myosin IIB (Biolegend, prb-445p; 1:500) were employed.

Chemically Fixed Sample Preparation and Transmission Electron Microscopy

Samples were fixed with 2.5% glutaraldehyde, 2% formaldehyde in 0.1 M sodium cacodylate buffer (pH 7.4) for 2 h at RT followed by post-fixation with ice-cold 1% OsO_4 in the same buffer for 2 h. After being stained en bloc with 0.5% uranyl acetate for 2 h or overnight at RT, samples were dehydrated with ethanol and propylene oxide and embedded in Poly/Bed 812 (Polyscience). Ultra-thin (70 nm) sections were double-stained with uranyl acetate and Reynold's lead citrate and examined under a JEOL JEM 1010 electron microscope at an accelerating voltage of 100 kV.

Downloaded by:
Washington State Univ Lib
134.121.42.92 - 12/20/2017 6:03:57 PM

High-Pressure Freezing, Freeze-Substitution, and Transmission Electron Microscopy

Main procedures of sample preparation and transmission electron microscopy (TEM) analysis followed previous descriptions [He et al., 2003] with minor modification to adapt with a different target tissue. The pregnant host animals were anesthetized by isoflorane, and urethral tissues at the proximal GT with thickness <100 μm were dissected quickly from live embryos and mounted flatly on the 100 μm depth specimen carriers for high-pressure freezing. Excess space of the carrier chamber was filled with 20% lipid-rich BSA (ALBUMAXI, Gibco) to remove air bubbles. Specimen were frozen within 310~380 ms under ~2,050 bar high-pressure with HPF-compact-01 (Wohlwend GmbH) to obtain a vitrified fixation. The time from embryo dissection to freezing was limited within 40 s to maintain better physiological conditions. Samples were transferred into screw-typed tubes containing 1% OsO_4 and 0.1% uranyl acetate in acetone in liquid nitrogen and were subsequently transferred into a Leica EM AFS2 for freeze-substitution. Substitution was programmed as –90°C for 24 h, –60°C for 10 h, and –30°C for 18 h. Temperatures increased slowly during each transition for more than 2 h. Samples were washed 3 times with pure acetone after warming up slowly to 4°C and were subsequently warmed up to RT. Urethral tissues were carefully separated from the carrier and infiltrated with Epoxy resin (SPI PON, DDSA, and NMA from SPI-CHEM). Polymerization of resin was achieved by warming at 45°C for 18–24 h and 60°C for 48 h. Sections of 70 nm were placed on 200 mesh fine bar hexagonal grids (Ted Pella, Inc.) coated with a formvar membrane. Positive staining was performed by 3% uranyl acetate in 70% methanol on ice for 7 min and SATO lead in RT for 2 min. Images were recorded with Tecnai G2 Spirit (FEI Corp., Eindhoven, The Netherlands) equipped with 4 k × 4 k CCD camera (Gatan Corp.).

Urethral Tissue Slice Culture and Time-Lapse Imaging

GTs with its proximal perineum tissue were dissected at E14.5, E15.5, and E16.5, rinsed, and embedded in 4% low melting agarose gel (Funakoshi, LM-01) with the distal tip of the GT vertically upward. Agarose gel-fixed tissues were sectioned into slices of 150 μm thickness with a Vibratome 7000 (Campden Instrument, Smz). Sections of urethral tissues in the proximal GT were analyzed. Paired urethral tissues were used for comparisons of different treatments. Rat-tail collagen I (BD3542236) was diluted to 2% and modulated at ~pH 7.3 with osmotic pressure by 10× PBS (Wako), charcoal-stripped FBS (Hyclone), 0.05 M NaOH. Urethral tissue slices were rinsed with 2% collagen gel and mounted on a 4-well glass bottom dish (Matsunami, D141400). The membrane of the cell culture inserts (MilliCell, PIHT30R48) was prepared into pieces of 9 mm diameter and rinsed with collagen gel. Urethral tissue slices were covered with the culture insert membrane for a flat mounting to the glass bottom. Collagen gel was fixed at 37°C for 10 min. Additional 100 μl of 2% collagen gel was added to the membrane and fixed at 37°C for 1 h. A volume of 200 μl F12 (Gibco) containing 20% charcoal-stripped FBS was added to each culture well. A physiological concentration of DHT (10^{-8} M) was used for the culture. Chemical inhibitors employed in the slice culture system were latrunculin A (Invitrogen) at 5 μM and jasplakinolide (Invitrogen) at 5 μM.

Spinning disk microscopies (Cell Voyager CV-1000, Yokogawa) with 60× oil lenses were employed for time-lapse imaging experiments. The 10 μm sample depth, ranging from 5 to 15 μm from the bottom of the tissue slice, was imaged to trace the actin dynamics and cell movement.

Imaging Analysis

Imaris (Bitplane) was utilized to modulate the brightness and contrast as well as make 10 μm 3D projections and snapshots at various time points for the time-lapse imaging analysis of Actin-venus indicator mice.

Imaris was also utilized to detect, track, and visualize cell displacement for the time-lapse imaging analysis of Lyn-Venus membrane indicator mice. Cells within 100 × 100 μm scope in the center of each image were tracked, and tracks were manually validated and corrected. Imaris was also applied to obtain quantitative data for the parameter of Track_Speed_Mean, Track_Displacement_Length, and Track_Length. Such parameters were analyzed in Microsoft Excel to represent the velocity and straightness of the cell movement. Graphpad prism5 was utilized to assemble the cell migratory data.

Results

Sexually Dimorphic F-Actin Pattern in Genital Development

Gross morphological sexual difference of the GT becomes initially evident in its ventral side at E16.5 [Suzuki et al., 2002; Yamada et al., 2003a]. The formation of the penile urethra extended into the male GT, whereas it was not formed in the female GT (Fig. 1A, B). Androgen signaling in the mesenchyme around the urethra (hereafter designated as UMCs) is essential for the formation of the penile urethra [Miyagawa et al., 2009; Suzuki et al., 2014]. Intriguingly, cellular morphology of UMCs was significantly different between sexes (Fig. 1C–F). Male UMCs mostly displayed elongated spindle-like cell shape (Fig. 1D, white arrows in Fig. 1F). In contrast, female UMCs showed more rounded morphology (Fig. 1C, white arrows in Fig. 1E).

Cytoskeletons support the dynamic changes of cellular morphology. We thus analyzed the cytoskeletal components of the UMCs. F-actin staining indicates the structural dynamics of actin filaments. Thin F-actin fibrils were observed in male UMCs (Fig. 1I, I', J; online suppl. Video1b; see www.karger.com/doi/10.1159/000477452 for all online suppl. material). On the other hand, a prominently differential pattern of F-actin was observed in female UMCs. F-actin was accumulated into an intensely stained prominent granulation reaching to 2–6 μm in diameter. Such accumulation projected thick fibrils out from the central granule (Fig. 1G, G', H; online suppl. Video1a). Moreover, one UMC appeared to possess one such F-actin accumulation based on its number relative to the nuclei number of the UMCs (No. of accumula-

Downloaded by:
Washington State Univ Lib
134.121.42.92 - 12/20/2017 6:03:57 PM

tions/no. of nuclei = 0.98 ± 0.09; 420 nuclei were counted, n = 6) (data not shown). Vimentin is one of the major components of intermediate filaments in mesenchymal cells, and α-tubulin is one of components of the subunit of the microtubule. Contrary to the prominent sexual differences of F-actin, neither the intermediate filaments nor the microtubule showed obvious sexual differences in UMCs (online suppl. Fig. 1A–H). These results suggest that the sexually dimorphic patterns of F-actin are associated with the dimorphic cellular shapes of UMCs. Next, we investigated sequentially the formation of F-actin assembly from E12.5 to postnatal day 35 (P35). Networks of F-actin fibrils were similarly observed in UMCs of both sexes earlier than E14.0 (Fig. 1K, L; data not shown). Sub-

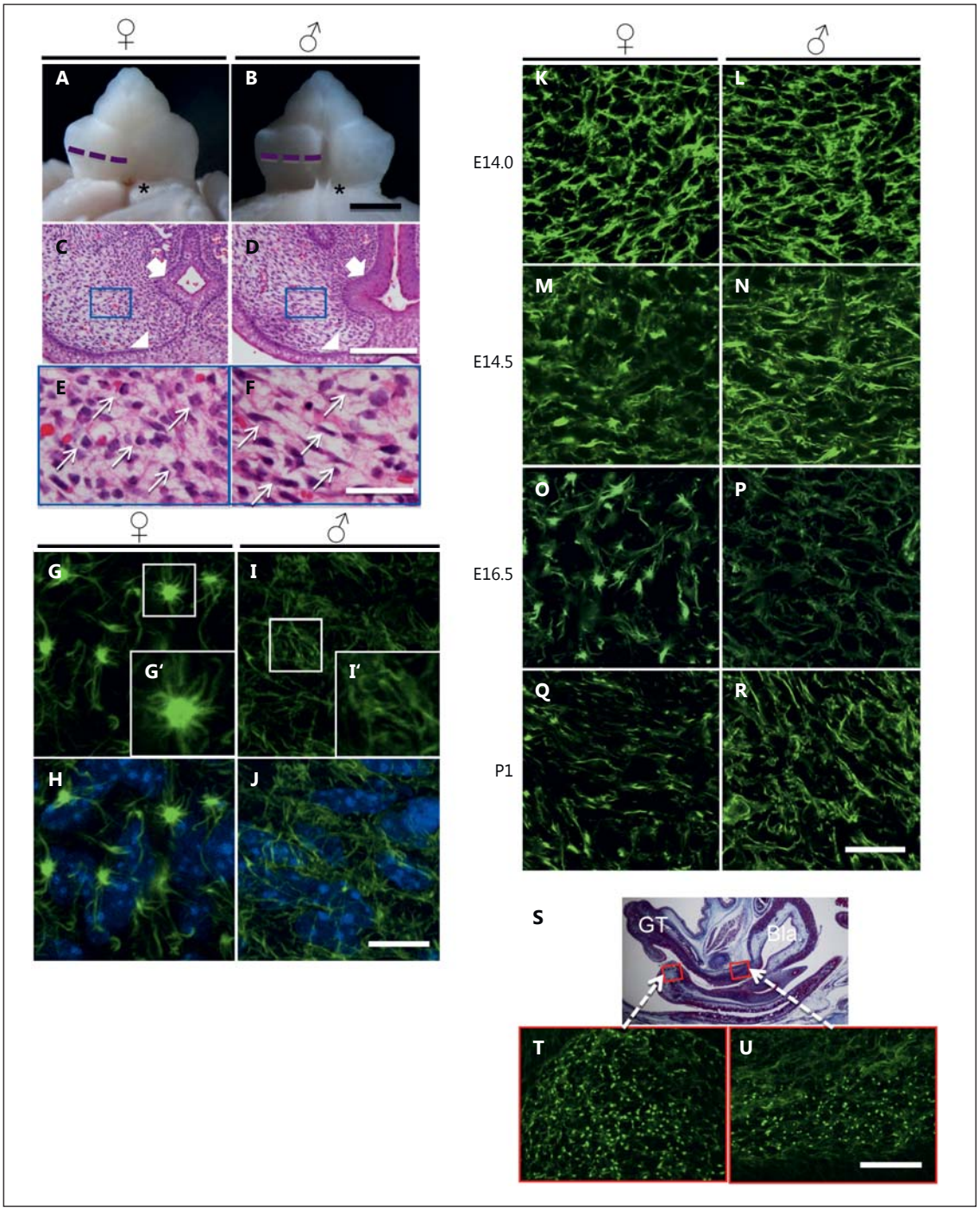

1

(For legend see next page.)

Downloaded by:
Washington State Univ Lib
134.121.42.92 - 12/20/2017 6:03:57 PM

sequently, F-actin was assembled into accumulated structures in female UMCs (Fig. 1M) in contrast to the thinner fibrils in male UMCs (Fig. 1N) at E14.5. The most prominent sexual difference of the F-actin assembly was observed between E16.5 and E17.5. Obvious F-actin accumulations were formed in the female UMCs (Fig. 1O). In contrast, much thinner F-actin fibrils developed in the male UMCs (Fig. 1P). Such sexually dimorphic patterns were less prominent at postnatal day 1 (P1) (Fig. 1Q, R). Thereafter, sexual differences of the F-actin pattern become gradually diminished during the postnatal stages (data not shown).

In order to gain insight into the sexual differences of F-actin patterns, we analyzed the F-actin assembly in other tissues of the body trunk and limbs at E16.5. Similar sexual differences could be hardly observed in the skin and the limb mesenchyme (data not shown). However, F-actin accumulations were prominently detected in 2 mesenchymal regions of the female reproductive tract. One location is the lower part of the urethral mesenchyme adjacent to the orifice (Fig. 1S, T), and the other positive region was the upper part of urogenital sinus (UGS) mesenchyme adjacent to the bladder neck region (Fig. 1S, U). This region corresponds to the prostatic budding site in the male urogenital sinus [Hayward et al., 1996] as also suggested by the presence of epithelial budding structures in the corresponding male region at E17.5 (data not shown). On the other hand, no such F-actin accumulation was detected in the urogenital tract of the male. Male mesenchymal cells presented filamentous pattern of F-actin in the corresponding regions (data not shown). Thus, formation of F-actin accumulation appears to be a female-specific feature in several reproductive tissues. We designate herein such accumulation as female-type F-actin accumulation (FTFA).

Androgen Signaling Modulates Progressive F-Actin Sexual Differentiation in UMCs

Androgen signaling regulates the masculinization of the reproductive tract [Yamada et al., 2003a; Wilhelm and Koopman, 2006; Welsh et al., 2008]. In order to verify the effect of androgen on F-actin assembly, time-lapse imaging systems were developed by using urethral tissue slice cultures. The actin fluorescent indicator mouse line, Actin-Venus [Abe et al., 2011], was employed to trace the actin dynamics of the UMCs at E14.5. Female UMCs developed FTFA-like structures within 12 h without DHT (Fig. 2B). They gradually achieved a large population of FTFA until 48 h (Fig. 2C–E), whose pattern was similar with the condition at E16.5 (Fig. 1O). The male UMCs developed FTFA without DHT within 36 h of culture (Fig. 2K–O). In contrast, male UMCs gradually formed thin F-actin fibrils in 2 days culture with DHT (Fig. 2P–T). Similar thin F-actin fibrils were also formed in the female UMCs under the treatment of DHT (Fig. 2F–J). Without DHT, F-actin developed into the FTFA regardless of the sex origins of the urethral tissue slices. These results suggest that DHT modulated F-actin patterning into thin fibrils.

To further confirm the involvement of androgen signaling for the formation of the F-actin pattern, we analyzed the GT of androgen receptor (AR) knockout (KO) mice. AR KO males also showed a similar F-actin phenotype like the WT female (online suppl. Fig. 2I, M). Furthermore, administration of DHT could not lead to the formation of the thin F-actin fibrils from FTFAs in AR KO male (online suppl. Fig. 2N, O, P). These results suggest that androgen signaling is essential for the modulation of the F-actin pattern.

DHT modulates the F-actin pattern from the accumulated into the fibrillar form in the female UMCs at E14.5

Fig. 1. F-actin sexual differentiation in genital mesenchymal cells. **A**, **B** Gross morphology of the genital tubercle (GT) in female (**A**) and male (**B**) mice at E16.5. Asterisks mark the orifice of the urethra in the female (**A**) and the fused urethra in the male in the proximal GT (**B**). Scale bar, 500 μm. **C–F** H & E staining of the urethral tissues at the proximal level of the GT indicated by dashed lines in **A** and **B**. **E**, **F** Urethral mesenchymal cells (UMCs) framed in **C** and **D**. Arrows show the urethral epithelium and arrowheads the ectodermal epithelium (**C**, **D**). Female UMCs mostly display rounded cell bodies (**C**, **E**, arrows) and male ones display elongated cell bodies (**D**, **F**, arrows). Scale bars, 150 μm (**C**, **D**) and 50 μm (**E**, **F**). **G**, **G′**, **I**, **I′** Maximum projection of 6 μm thickness confocal images of F-actin stained by phalloidin-Alexa488 in the UMCs. **G′**, **I′** Enlarged views of the framed area in **G** and **I**. **H**, **J** Merged images of F-actin with nuclei. Prominent F-actin accumulation with multiple fibrils projected out from the center in the female UMCs (**G**, **G′**, **H**). Thin F-actin fibrils are formed in the male UMCs (**I**, **I′**, **J**). Scale bar, 10 μm. **K–R** Time-course of F-actin sexual differentiation in the UMCs. F-actin patterns in UMCs show no obvious sexual differences between E14.0 female (**K**) and male (**L**). There is a partially accumulated pattern in female (**M**), and bundled fibrillar pattern in male (**N**) at E14.5, prominent F-actin accumulations in female (**O**) and thin fibrils in male (**P**) at E16.5, and a less accumulated pattern in female (**Q**) and less thin fibrils in male (**R**) at P1 compared to E16.5 female and male. Scale bar, 10 μm. **S–U** Spatial presence of F-actin accumulation. **S** Masson staining of the female urogenital system. Accumulated F-actin staining is present in the lower portion of the urethral mesenchyme under the perineum region (**T**) and in the upper portion of the urogenital-sinus mesenchyme in the bladder (Bla) neck region (**U**). Scale bar, 50 μm.

Downloaded by:
Washington State Univ Lib
134.121.42.92 - 12/20/2017 6:03:57 PM

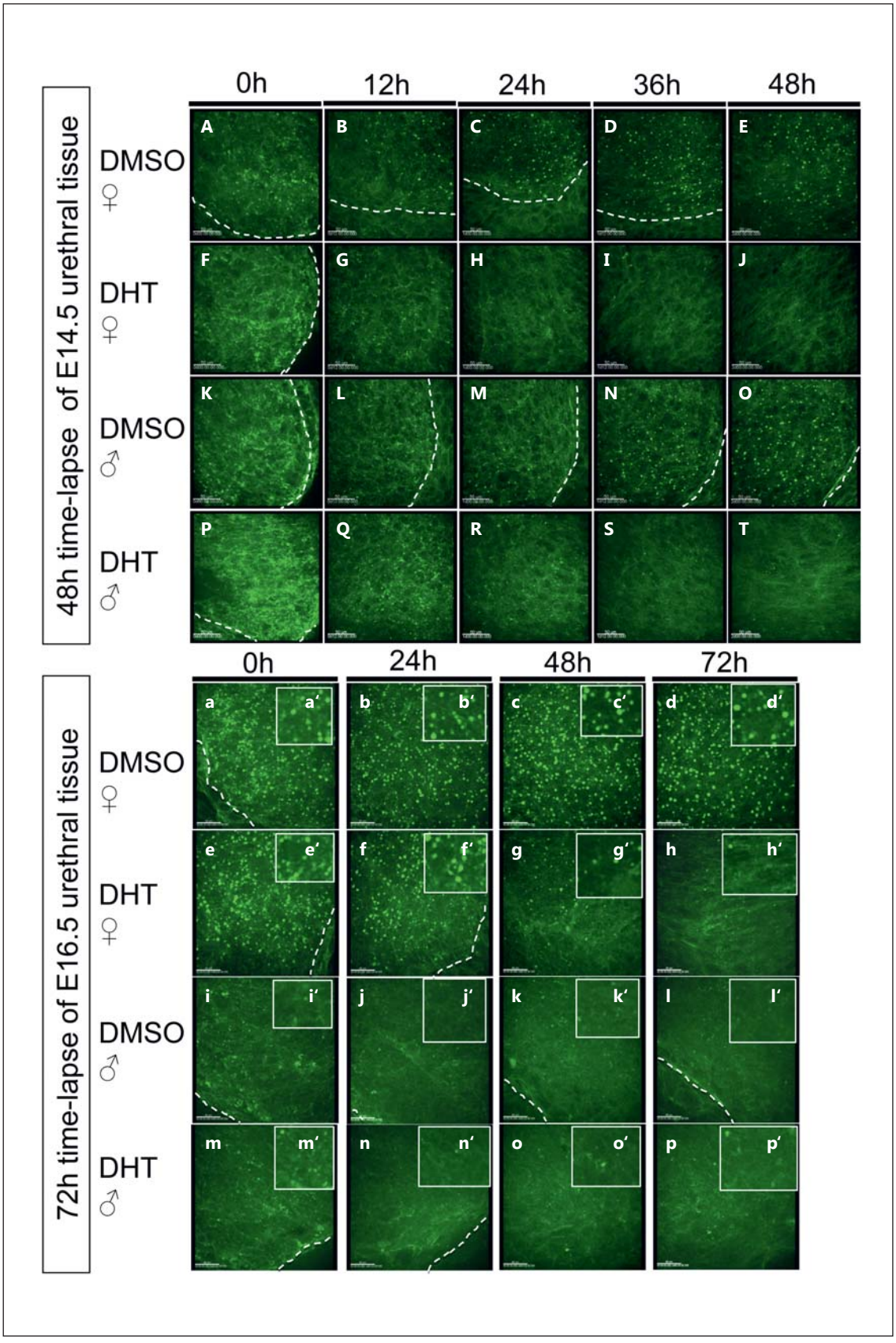

2

(For legend see next page.)

Downloaded by:
Washington State Univ Lib
134.121.42.92 - 12/20/2017 6:03:57 PM

within 24 h (Fig. 2G, H). One day later, namely at E15.5, a longer time was necessary for such DHT-induced modulation of the F-actin pattern in female UMCs (online suppl. Fig. 2F, G, H). These results suggest that the duration of androgen exposure for modulating the F-actin pattern may depend on the developmental stage. To confirm the possibility, we evaluated the timespan to reverse the F-actin sexual pattern of E16.5 specimens. Some FTFAs still remained longer than 48 h of DHT treatment in female UMCs at E16.5 (Fig. 2g, g', h, h'). In the case of male UMCs, approximately 24 h were enough to form FTFA-like structures at E14.5 without DHT (Fig. 2M). However, almost no F-actin accumulations were formed even after 72 h culture of UMCs at E16.5 without DHT (Fig. 2l, l').

Dimorphic Assemblies of the Extracellular Matrix in UMCs

In order to get insights on the sexually dimorphic pattern of F-actin, we analyzed the subcellular localization of the F-actin structures by TEM. F-actin-like electron-dense structures were observed as the mass structure in the cytoplasm of female UMCs (Fig. 3A, area circled by white dashed line in Fig. 3C). Bundle-like structures were observed adjacent to the plasma membrane of the male UMCs (Fig. 3B, arrowheads in Fig. 3D). The physiological status of the cell can be preserved by fast cryo-fixation with high-pressure freezing followed by dehydration through freeze-substitution to reduce extraction of cellular contents [He et al., 2003; McDonald, 2014]. To further characterize dimorphic F-actin assembly, such samples were analyzed by TEM. Electron-dense mass structure was similarly observed in female UMCs (area circled by white dashed lines in Fig. 3E, G). Such FTFA-like structures occupied a large portion of cytoplasmic space, almost devoid of other subcellular organelles inside the FTFA (Fig. 3E, G). Visible F-actin bundles in male UMCs were likely formed adjacent to the plasma membrane (Fig. 3F, H, arrowheads). Such membranous localization of F-actin in the male may promote the physical interaction of the UMC with the ECM in the male.

Fibronectin, one of the key ECM components of mesenchymal fibroblasts, transduces mechanical forces between the intracellular cytoskeleton and the ECM through its membrane receptor, integrin α5β1 [Pankov and Yamada, 2002]. Fibronectin was assembled into fibrils, which co-aligned with the F-actin fibrils in the male UMCs (Fig. 4C, D, I, J, L; arrows), whereas fibronectin represented a patchy and non-linearized form in female UMCs (Fig. 4A, B, E, F, H). Prominent staining of integrin α5 was detected between the co-aligned fibrils of intracellular F-actin and extracellular fibronectin in male UMCs (Fig. 4K, L; arrows). In contrast, integrin α5 staining was barely observed between scarcely existing F-actin- and fibronectin-fibrils in the female UMCs (Fig. 4G, H; arrows). These results suggest the presence of more associations of F-actin structures with ECM in the male UMCs.

DHT Regulates Coordinated and Efficient Migration of UMCs

Dimorphic assemblies of both F-actin and the ECM indicated that there may be sexually different cellular behaviors of UMCs. To investigate this possibility, we analyzed the cellular behaviors of UMCs. Some UMCs migrated from the GT tissue slice into the collagen gel after 48 h culture of E14.5 specimens. We traced the behaviors of such UMCs derived from Actin-Venus indicator mice. Female UMCs moved randomly and barely contacted each other (online suppl. Video 2a). In contrast, female

Fig. 2. Stage-dependent regulation of F-actin sexual differentiation by androgen through the time-lapse imaging analyses of Actin-Venus indicator mice. **A–T** Imaging snapshots of E14.5 urethral tissue slices of female (**A–J**) and male (**K–T**) cultured with (**F–J**, **P–T**) or without (**A–E**, **K–O**) 10^{-8} M dehydrotestosterone (DHT) in 48 h. Female UMCs at E14.5 develop some F-actin accumulations within 12 h (**B**) and gradually achieve a large population of F-actin accumulation within 48 h (**C–E**) without DHT (DMSO vehicle control). Female UMCs at E14.5 gradually develop thin F-actin fibrils with DHT (**F–J**). Male UMCs at E14.5 develop a few F-actin accumulations at 24 h (**M**) and achieve a large population of F-actin accumulations at 48 h without DHT (**O**). Male UMCs gradually develop thin F-actin fibrils with DHT (**P–T**). **a–d** Imaging snapshots of E16.5 female (**a–h**) and male (**i–p**) urethral tissue slices cultured with (**e–h**, **m–p**) or without (**a–d**, **i–l**) 10^{-8} M DHT in 72 h. **a'–p'** Enlarged views of the central areas of **a–p**. Prominent F-actin accumulations of E16.5 female UMCs at 0 h (**a**, **a'**) were maintained in 72 h culture without DHT (**b**, **b'–d**, **d'**). Prominent F-actin accumulations of E16.5 female UMCs at 24 h (**e**, **e'**) are gradually reformed into thin fibrils (**f**, **f'–h**, **h'**), and a few remnants of F-actin accumulation remain at 72 h (**h**, **h'**) in the culture with DHT. Thin F-actin fibrils in E16.5 male UMCs at 0 h (**i**, **i'**) were basically maintained in the 72 h culture without DHT (**j**, **j'–l**, **l'**). Thin F-actin fibrils of E16.5 male UMCs (**m**, **m'**) were maintained in the 72 h culture with DHT (**n**, **n'–p**, **p'**). All images are Z-stalk projections of 10 μm thickness (11 slices, step-height 1 μm). Dashed lines, epithelial mesenchymal border. Scale bars, 50 μm.

Downloaded by:
Washington State Univ Lib
134.121.42.92 - 12/20/2017 6:03:57 PM

UMCs associated and tended to migrate as a group when treated with DHT (online suppl. Video 2b). Male UMCs showed coordinated movements similar with the female UMCs in a DHT-treated condition (online suppl. Video 2d). However, male UMCs without DHT treatment migrated randomly and discretely (online suppl. Video 2c). These results indicate that DHT may promote coordinated cell behaviors of UMCs.

To further investigate the sexual differences of the migratory behaviors of the UMCs, Lyn-Venus membrane indicator mice [Abe et al., 2011] were employed to trace the individual cell movement in urethral tissue slices (Fig. 5; online suppl. Video 3). Male UMCs mostly migrated to the direction of the urethral epithelium (indicated as red line in Fig. 5 A–D), especially with DHT (Fig. 5B, D). However, female UMCs mostly migrated in

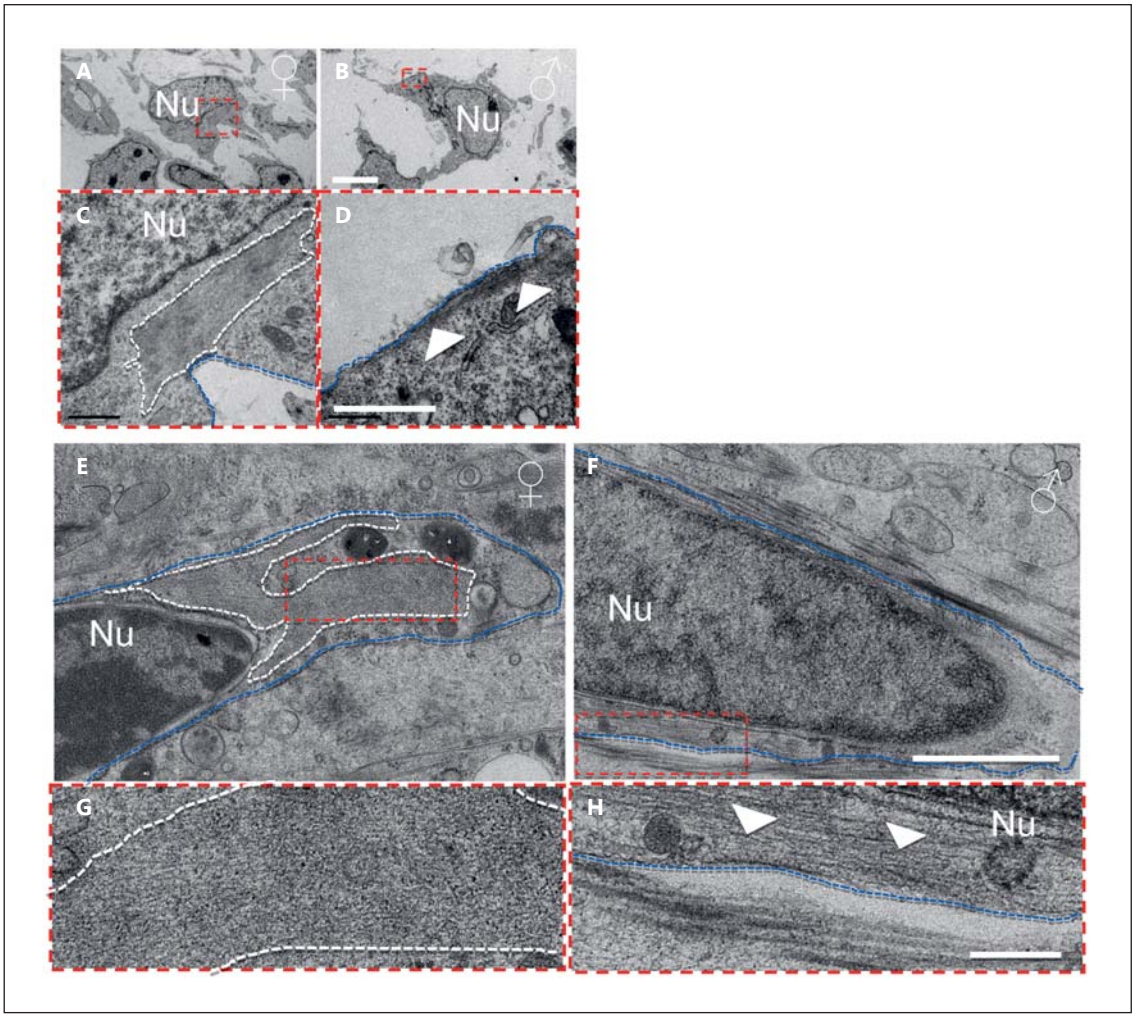

Fig. 3. Dimorphic assemblies of actin filament revealed by transmission electron microscopy (TEM). **A–D** Chemical-fixed electron microscopy showed the sex-differentiated status of F-actin. An electron-dense mass structure located in the cytoplasm was observed in the female UMCs (**C**, encircled by a white dashed line). The most prominent bundle-like actin structure was observed underneath the plasma membrane (**B**, **D**). The arrowheads point to F-actin structures in male UMCs (**D**), and blue dashed lines show the plasma membranes. Nu, Nucleus. Scale bars, 5 μm (**A**, **B**) and 1 μm (**C**, **D**). **E–H** High-pressure freezing, freeze substitution, and electron microscopy showed sex-differentiated status of F-actin in UMCs. The F-actin structure occupied a large portion of the cytoplasmic area (encircled by white dashed lines in **E** and enlarged in **G**), devoid of other cellular organelles inside the FTFA-like structure in the female UMC (**E**, **G**). F-actin bundles are located adjacent to the plasma-membrane in the male UMC (**F**, **H**). Arrowheads point to F-actin structures in male UMCs (**H**), and blue dashed lines show the plasma membranes. Nu, Nucleus. Scale bars, 1 μm (**E**, **F**) and 200 nm (**G**, **H**).

Downloaded by:
Washington State Univ Lib
134.121.42.92 - 12/20/2017 6:03:57 PM

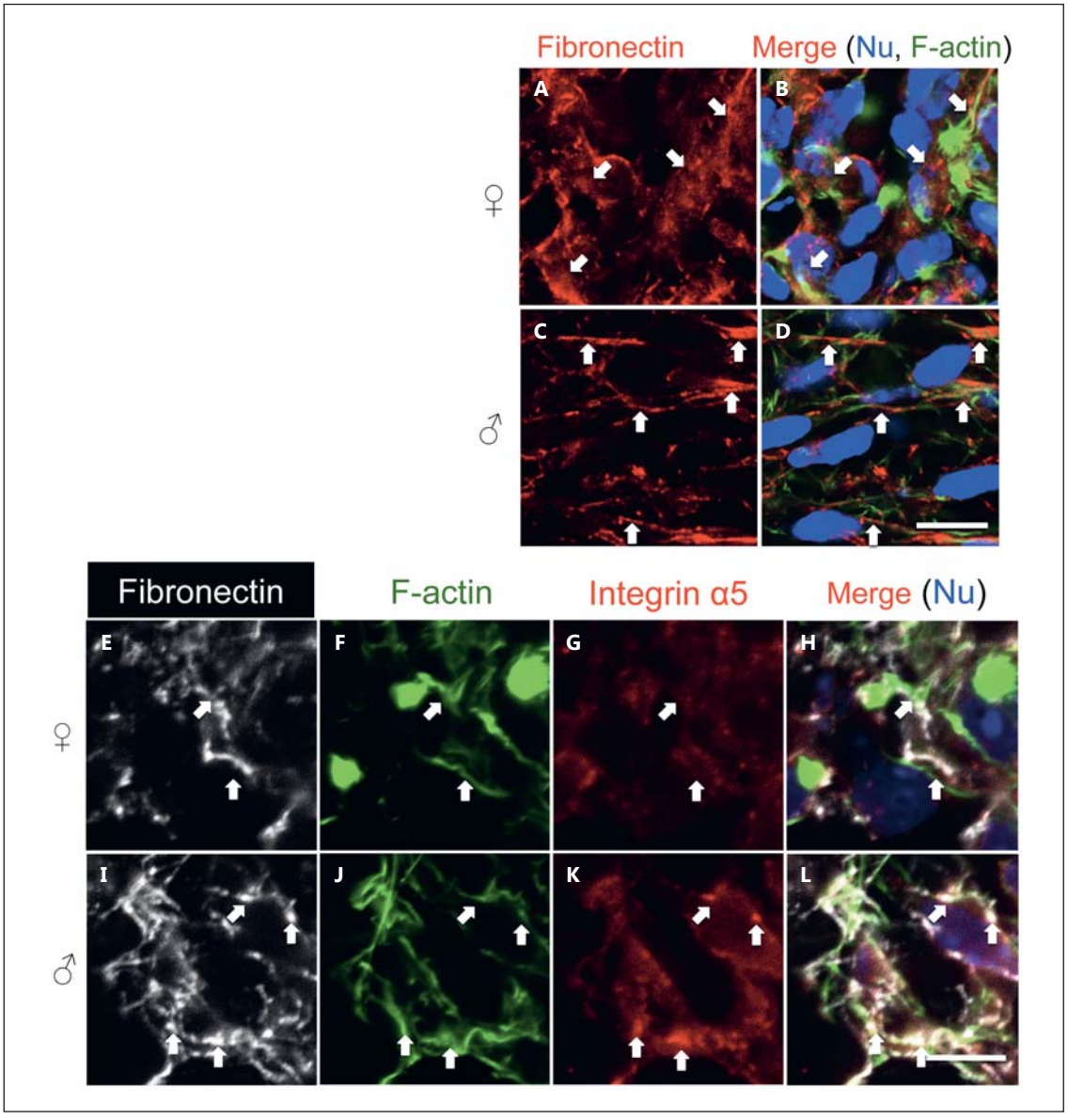

Fig. 4. More prominent co-alignment of fibronectin and F-actin in male UMCs. **A–D** Expression pattern of fibronectin of E16.5 UMCs. **B**, **D** Merged images of fibronectin (**A**, **C**) with F-actin (green) and nucleus (blue). Fibronectin presented a patchy and disorganized form (**A**), with few thick fibrils colocalized with FTFA in female UMCs (**B**). Fibronectin was assembled into fibrils (**C**), which co-aligned with the F-actin fibrils in male UMCs (**D**). Arrows show selective sites of fibronectin distribution. Scale bar, 10 μm. Immuno-fluorescent staining of fibronectin (**E**, **I**), F-actin (**F**, **J**), integrin α5 (**G**, **K**), and merged image of 3 fluorescence stainings with nucleus staining (**H**, **L**). Fibronectin of male UMCs (**I**) present a mostly fibrillar phenotype, co-aligned with intracellular F-actin (**J**, **L**), and there is prominent clustering of integrin α5 between the fibrils of F-actin and fibronectin as indicated by arrows (**K**, **L**). Fibronectin of female UMCs present a patchy form (**E**), barely colocalized with F-actin structures (**F**, **H**), and there is no prominent integrin α5 staining between the fibrils of fibronectin and F-actin as indicated by arrows (**G**, **H**). Scale bar, 5 μm.

random directions (Fig. 5A). The order of moving velocity of UMCs from low to high was female without DHT, female with DHT, male without DHT, and male with DHT (Fig. 5E). Straightness represents the ratio of displacement to the total migrating distance, which indicates the efficiency of the cell movement in one direction. The order of straightness was female without DHT, female with DHT, male without DHT, and male with DHT as the

Sex Dev 2017;11:190–202
DOI: 10.1159/000477452

Downloaded by:
Washington State Univ Lib
134.121.42.92 - 12/20/2017 6:03:57 PM

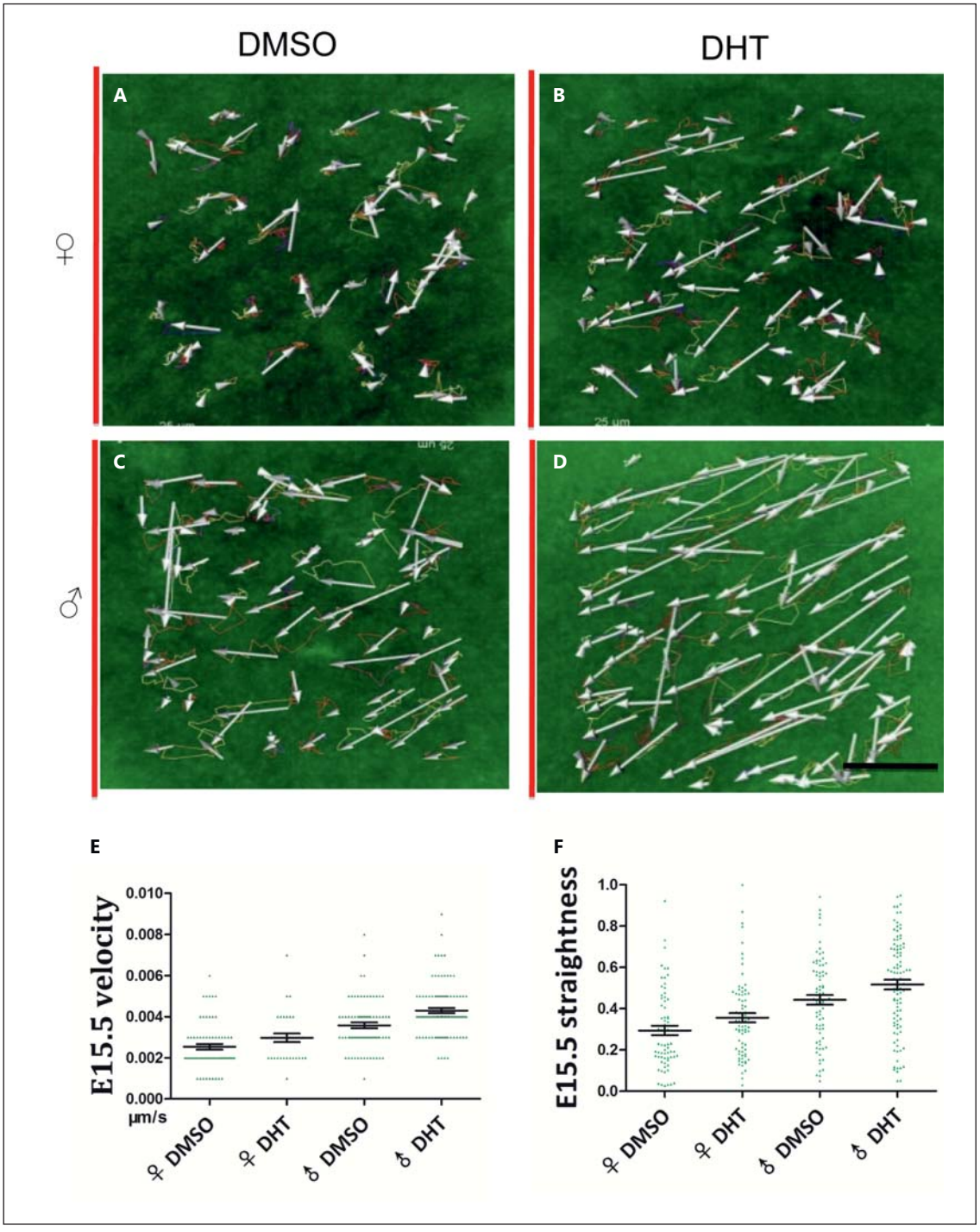

Fig. 5. Androgen regulates more rapid and directional movement of the UMCs. Movement of UMCs in 12-h time-lapse imaging of E15.5 urethral tissue slices from Lyn-Venus membrane indicator mice was traced by Imaris software. Moving route of the UMCs of female (**A**, **B**) or male (**C**, **D**) with (**B**, **D**) or without (**A**, **C**) DHT is displayed by both moving tracks (colored curved lines) and displacement (arrows). Scale bar, 25 μm. The urethral epithelium is arranged to the left side of urethral tissue slices and is indicated by red lines in **A–D**. Female UMCs without androgen treatment migrate randomly in all directions (**A**). Male UMCs with androgen treatment migrate coordinately to the urethral epithelium (**D**). **E** Velocity and **F** straightness (displacement/length of moving tracks) of UMCs movement are displayed with dispersing point graph. Average velocities of the cells are as follows: female DMSO = 0.0025 μm/s; female DHT = 0.0028 μm/s; male DMSO = 0.0036 μm/s; male DHT = 0.0043 μm/s. Average values of straightness for each group are as follows: female DMSO = 0.29; female DHT = 0.36; male DMSO = 0.44; male DHT = 0.52.

Downloaded by:
Washington State Univ Lib
134.121.42.92 - 12/20/2017 6:03:57 PM

highest (Fig. 5F), which showed a similar tendency with the order of moving velocity. These results indicate that DHT may induce the more efficient and coordinated mobility of the UMCs to the urethral epithelium.

Discussion

Androgen Regulates the Sexually Dimorphic F-Actin Pattern

The current results indicate that the F-actin pattern in UMCs shows sexual differences and that androgen signaling is involved in the formation of such pattern. AR function in the mesenchyme is indispensable for fetal sexual differentiation of genital organs in the reproductive tract [Miyagawa et al., 2009]. AR was expressed in the UMCs more prominently in the male between E14.5 to E16.5 [Miyagawa et al., 2009; data not shown]. Secretion of testicular androgen from E13.0 initiates activities of androgen signaling in male embryos [O'Shaughnessy et al., 2006; Dean et al., 2012]. The sexually dimorphic F-actin assemblies in UMCs became initially distinguishable at E14.5, evident at E15.5 and E16.5. The critical time window for the dimorphic development of the GT in mice is reported from E15.5 to E16.5 [Miyagawa et al., 2009]. Sexually dimorphic F-actin patterns were formed around the timing of the MPW. A current study showed that the sexually dimorphic pattern of F-actin was reversible. However, the duration to accomplish sex-reversal patterns of F-actin appeared to depend on the developmental stage. Longer exposure time to modulate androgen signaling was necessary to reverse the female F-actin pattern in late stage (E16.5, more than 3 days) than in earlier stages (E14.5, within 1 days; E15.5, within 2 days). These results suggest that the mesenchymal response to androgen may be different in each stage. Of note, hypospadias-like phenotypes could be induced by anti-androgenic chemicals in the early and mid-stages of the MPW but not in the late MPW [Welsh et al., 2008]. Further analyses are required to understand the correlation between abnormal urethral formation and defects of the F-actin pattern formation.

Sexually dimorphic F-actin patterns were formed not only in the UMCs but also in the mesenchyme of some other embryonic genital regions, including the UGS adjacent to the bladder neck region and the anterior portion of the perineum. These 2 regions also show androgen-dependent masculinization such as prostate budding and perineum elongation. Furthermore, sexually dimorphic patterns of F-actin in the above reproductive tissues were formed at similar embryonic stages in the MPW. Taken together, the spatio-temporal programs of the formation of sexually dimorphic F-actin patterns may contribute to the sexual differentiation of several reproductive tissues.

Sexually Dimorphic F-Actin Patterns Possibly Regulate Distinct Behaviors of UMCs

The F-actin organizations provide a cellular basis for the contractive machineries of the cell to assemble the ECM [Ennomani et al., 2016]. The prominent presence of FTFA may attenuate the membranous distribution of F-actin networks, which may decrease the ability of the cell to associate with the ECM. Such a situation might lead to a poor assembly of the ECM in female UMCs.

Fibronectin binds to the cell membrane by its receptor, integrin α5β1, and regulates the assembly of several other ECM proteins [Pankov and Yamada, 2002; Yamada et al., 2003b]. The expression of integrin α5 between co-aligned F-actin and fibronectin fibrils indicated close associations of fibronectin and F-actin in male UMCs. Such association of F-actin fibrils with fibronectin may transduce mechanical properties from the cell to the ECM facilitating the assembly of the ECM adjacent to the plasma membrane of male UMCs [Yamada et al., 2003b; Alberts, 2008; Leiss et al., 2008]. Well-assembled ECM aligning along cell bodies might promote cellular behaviors of male UMCs in favor of their directional movement.

DHT promoted coordinated cell migration of UMCs in isolated collagen gel environments. Moreover, UMCs migrated more efficiently toward the urethral epithelium of the urethral tissue slices with DHT treatment. Such migration appeared to occur synergistically with a DHT-induced alteration of F-actin patterns. Furthermore, actin polymerization toxins, such as latrunculin A and jasplakinolide, diminished the F-actin sexual patterns and abolished the mobility of UMCs at the same time (data not shown). Thus, sexually dimorphic patterns of F-actin could play roles in the coordinated directional movement under androgen actions. The formation of the penile urethra involves a dynamic rearrangement of the urethral epithelium, such as the fusion of the urethral plate and the internalization of the urethral tube in the glans. Coordinated migration of UMCs toward the urethral epithelium might positively contribute to such active morphogenetic processes.

Advances in genetic and molecular studies promote the understanding of the mechanism of genital sexual differentiation. Several genes have been identified as essential regulators of male- and female-type reproductive organ formation [Miyagawa et al., 2009; Chen et al., 2010; Chen et al., 2011; Suzuki et al., 2014]. However, the cel-

Downloaded by:
Washington State Univ Lib
134.121.42.92 - 12/20/2017 6:03:57 PM

lular level of differentiation, particularly mesenchymal characters in the male- and female-type genital organ formation processes remain unelucidated. Dimorphic F-actin assembly in genital organogenesis might be one of the cellular mechanisms for sexual differentiation of reproductive tissues. Further studies are required to reveal the molecular mechanisms of sexually different assemblies of F-actin regulated by androgen.

Acknowledgments

We thank Drs Benjamin Odermatt, Robert S. Adelstein, Toru Miyazaki, Takashi Seki, Jun Hatakeyama, Nan Tang for their invaluable support, and T. Iba for assistance. We also thank CDB laboratory for Animal Resources and Genetic Engineering for the source of the indicator mice. This work was supported by the Japan Society for the Promotion of Science KAKENHI Grant Numbers 15H04300, 15K15403 and 15K10647, also by China MOST (973 programs, 2011CB812502, 2014CB849902), and the Beijing Municipal Government.

Statement of Ethics

All experimental procedures and protocols were approved by the Committee on the Animal Research at the Kumamoto University (B22-198, A23-076), Wakayama Medical University (798), Japan, and by National Institute of Biological Science, Beijing, China (0013).

Disclosure Statement

The authors have no conflicts of interest to declare.

References

Abe T, Kiyonari H, Shioi G, Inoue K, Nakao K, et al: Establishment of conditional reporter mouse lines at rosa26 locus for live cell imaging. Genesis 49:579–590 (2011).

Alberts B: Molecular Biology of the Cell, ed 5 (Garland Science, New York 2008).

Araki K, Imaizumi T, Okuyama K, Oike Y, Yamamura K: Efficiency of recombination by cre transient expression in embryonic stem cells: comparison of various promoters. J Biochem 122:977–982 (1997).

Blanchoin L, Boujemaa-Paterski R, Sykes C, Plastino J: Actin dynamics, architecture, and mechanics in cell motility. Physiol Rev 94:235–263 (2014).

Chen H, Yong W, Hinds TD Jr, Yang Z, Zhou Y, et al: Fkbp52 regulates androgen receptor transactivation activity and male urethra morphogenesis. J Biol Chem 285:27776–27784 (2010).

Chen N, Harisis GN, Farmer P, Buraundi S, Sourial M, et al: Gone with the wnt: the canonical wnt signaling axis is present and androgen dependent in the rodent gubernaculum. J Pediatr Surg 46:2363–2369 (2011).

Cunha GR, Sinclair A, Risbridger G, Hutson J, Baskin LS: Current understanding of hypospadias: relevance of animal models. Nat Rev Urol 12:271–280 (2015).

Dean A, Smith LB, Macpherson S, Sharpe RM: The effect of dihydrotestosterone exposure during or prior to the masculinization programming window on reproductive development in male and female rats. Int J Androl 35:330–339 (2012).

Ennomani H, Letort G, Guerin C, Martiel JL, Cao W, et al: Architecture and connectivity govern actin network contractility. Curr Biol 26:616–626 (2016).

Friedl P, Wolf K: Plasticity of cell migration: a multiscale tuning model. J Cell Biol 188:11–19 (2010).

Grinnell F: Fibroblast mechanics in three-dimensional collagen matrices. J Bodyw Mov Ther 12:191–193 (2008).

Haraguchi R, Motoyama J, Sasaki H, Satoh Y, Miyagawa S, et al: Molecular analysis of coordinated bladder and urogenital organ formation by hedgehog signaling. Development 134:525–533 (2007).

Hayward SW, Baskin LS, Haughney PC, Foster BA, Cunha AR, et al: Stromal development in the ventral prostate, anterior prostate and seminal vesicle of the rat. Acta Anat 155:94–103 (1996).

He W, Cowin P, Stokes DL: Untangling desmosomal knots with electron tomography. Science 302:109–113 (2003).

Heisenberg CP, Bellaiche Y: Forces in tissue morphogenesis and patterning. Cell 153:948–962 (2013).

Leiss M, Beckmann K, Giros A, Costell M, Fassler R: The role of integrin binding sites in fibronectin matrix assembly in vivo. Curr Opin Cell Biol 20:502–507 (2008).

Luo W, Yu CH, Lieu ZZ, Allard J, Mogilner A, et al: Analysis of the local organization and dynamics of cellular actin networks. J Cell Biol 202:1057–1073 (2013).

Manson JM, Carr MC: Molecular epidemiology of hypospadias: review of genetic and environmental risk factors. Birth Defects Res A Clin Mol Teratol 67:825–836 (2003).

McDonald KL: Rapid embedding methods into epoxy and Lr White resins for morphological and immunological analysis of cryofixed biological specimens. Microsc Microanal 20:152–163 (2014).

Miyagawa S, Satoh Y, Haraguchi R, Suzuki K, Iguchi T, et al: Genetic interactions of the androgen and wnt/beta-catenin pathways for the masculinization of external genitalia. Mol Endocrinol 23:871–880 (2009).

Murashima A, Miyagawa S, Ogino Y, Nishida-Fukuda H, Araki K, et al: Essential roles of androgen signaling in Wolffian duct stabilization and epididymal cell differentiation. Endocrinology 152:1640–1651 (2011).

Ogi H, Suzuki K, Ogino Y, Kamimura M, Miyado M, et al: Ventral abdominal wall dysmorphogenesis of *msx1/msx2* double-mutant mice. Anat Rec A Discov Mol Cell Evol Biol 284:424–430 (2005).

O'Shaughnessy PJ, Baker PJ, Johnston H: The foetal Leydig cell– differentiation, function and regulation. Int J Androl 29:90–95; discussion 105–108 (2006).

Pankov R, Yamada KM: Fibronectin at a glance. J Cell Sci 115:3861–3863 (2002).

Sato T, Matsumoto T, Kawano H, Watanabe T, Uematsu Y, et al: Brain masculinization requires androgen receptor function. Proc Natl Acad Sci USA 101:1673–1678 (2004).

Downloaded by:
Washington State Univ Lib
134.121.42.92 - 12/20/2017 6:03:57 PM

Suzuki H, Suzuki K, Yamada G: Systematic analyses of murine masculinization processes based on genital sex differentiation parameters. Dev Growth Differ 57:639–647 (2015).
Suzuki H, Matsushita S, Suzuki K, Yamada G: 5alpha-dihydrotestosterone negatively regulates cell proliferation of the periurethral ventral mesenchyme during urethral tube formation in the murine male genital tubercle. Andrology 5:146–152 (2017).
Suzuki K, Ogino Y, Murakami R, Satoh Y, Bachiller D, Yamada G: Embryonic development of mouse external genitalia: insights into a unique mode of organogenesis. Evol Dev 4: 133–141 (2002).
Suzuki K, Numata T, Suzuki H, Raga DD, Ipulan LA, et al: Sexually dimorphic expression of Mafb regulates masculinization of the embryonic urethral formation. Proc Natl Acad Sci USA 111:16407–16412 (2014).
Welsh M, Saunders PT, Fisken M, Scott HM, Hutchison GR, et al: Identification in rats of a programming window for reproductive tract masculinization, disruption of which leads to hypospadias and cryptorchidism. J Clin Invest 118:1479–1490 (2008).
Welsh M, Suzuki H, Yamada G: The masculinization programming window. Endocr Dev 27: 17–27 (2014).
Wilhelm D, Koopman P: The makings of maleness: towards an integrated view of male sexual development. Nat Rev Genet 7:620–631 (2006).
Yamada G, Satoh Y, Baskin LS, Cunha GR: Cellular and molecular mechanisms of development of the external genitalia. Differentiation 71:445–460 (2003a).
Yamada KM, Pankov R, Cukierman E: Dimensions and dynamics in integrin function. Braz J Med Biol Res 36:959–966 (2003b).
Yong W, Yang Z, Periyasamy S, Chen H, Yucel S, et al: Essential role for co-chaperone Fkbp52 but not Fkbp51 in androgen receptor-mediated signaling and physiology. J Biol Chem 282: 5026–5036 (2007).

Downloaded by:
Washington State Univ Lib
134.121.42.92 - 12/20/2017 6:03:57 PM